Cell Stem Cell
Short Article

Modeling Alzheimer's Disease with iPSCs Reveals Stress Phenotypes Associated with Intracellular Aβ and Differential Drug Responsiveness

Takayuki Kondo,[1,2,7] Masashi Asai,[7,9,10] Kayoko Tsukita,[1,7] Yumiko Kutoku,[11] Yutaka Ohsawa,[11] Yoshihide Sunada,[11] Keiko Imamura,[1] Naohiro Egawa,[1] Naoki Yahata,[1,7] Keisuke Okita,[1] Kazutoshi Takahashi,[1] Isao Asaka,[1] Takashi Aoi,[1] Akira Watanabe,[1] Kaori Watanabe,[7,10] Chie Kadoya,[7,10] Rie Nakano,[7,10] Dai Watanabe,[3] Kei Maruyama,[9] Osamu Hori,[12] Satoshi Hibino,[13] Tominari Choshi,[13] Tatsutoshi Nakahata,[1] Hiroyuki Hioki,[4] Takeshi Kaneko,[4] Motoko Naitoh,[5] Katsuhiro Yoshikawa,[5] Satoko Yamawaki,[5] Shigehiko Suzuki,[5] Ryuji Hata,[14] Shu-ichi Ueno,[15] Tsuneyoshi Seki,[16] Kazuhiro Kobayashi,[16] Tatsushi Toda,[16] Kazuma Murakami,[6] Kazuhiro Irie,[6] William L. Klein,[17] Hiroshi Mori,[18] Takashi Asada,[19] Ryosuke Takahashi,[2] Nobuhisa Iwata,[7,10,*] Shinya Yamanaka,[1,8] and Haruhisa Inoue[1,7,8,*]
[1]Center for iPS Cell Research and Application (CiRA)
[2]Department of Neurology, Graduate School of Medicine
[3]Department of Biological Sciences, Graduate School of Medicine and Department of Molecular and Systems Biology, Graduate School of Biostudies
[4]Department of Morphological Brain Science, Graduate School of Medicine
[5]Department of Plastic and Reconstructive Surgery, Graduate School of Medicine
[6]Organic Chemistry in Life Science, Division of Food Science and Biotechnology, Graduate School of Agriculture
Kyoto University, Kyoto 606-8507, Japan
[7]Core Research for Evolutional Science and Technology (CREST)
[8]Yamanaka iPS Cell Special Project
Japan Science and Technology Agency (JST), Saitama 332-0012, Japan
[9]Department of Pharmacology, Faculty of Medicine, Saitama Medical University, Saitama 350-0495, Japan
[10]Laboratory of Molecular Biology and Biotechnology, Department of Molecular Medicinal Sciences, Graduate School of Biomedical Sciences, Nagasaki University, Nagasaki 852-8521, Japan
[11]Department of Neurology, Kawasaki Medical School, Okayama 701-0192, Japan
[12]Department of Neuroanatomy (Biotargeting), Kanazawa University Graduate School of Medical Sciences, Ishikawa 920-8640, Japan
[13]Faculty of Pharmacy and Pharmaceutical Sciences, Fukuyama University, Hiroshima 729–0292, Japan
[14]Department of Functional Histology
[15]Department of Psychiatry
Ehime University Graduate School of Medicine, Ehime 791-0295, Japan
[16]Division of Neurology/Molecular Brain Science, Kobe University Graduate School of Medicine, Kobe, Hyogo 650-0017, Japan
[17]Department of Neurobiology, Northwestern University, Evanston, IL 60208, USA
[18]Department of Neuroscience, Graduate School of Medicine, Osaka City University, Osaka 545-8585, Japan
[19]Department of Neuropsychiatry, Institute of Clinical Medicine, University of Tsukuba, Ibaraki 305-8577, Japan
*Correspondence: haruhisa@cira.kyoto-u.ac.jp (H.I.), iwata-n@nagasaki-u.ac.jp (N.I.)
http://dx.doi.org/10.1016/j.stem.2013.01.009

SUMMARY

Oligomeric forms of amyloid-β peptide (Aβ) are thought to play a pivotal role in the pathogenesis of Alzheimer's disease (AD), but the mechanism involved is still unclear. Here, we generated induced pluripotent stem cells (iPSCs) from familial and sporadic AD patients and differentiated them into neural cells. Aβ oligomers accumulated in iPSC-derived neurons and astrocytes in cells from patients with a familial amyloid precursor protein (APP)-E693Δ mutation and sporadic AD, leading to endoplasmic reticulum (ER) and oxidative stress. The accumulated Aβ oligomers were not proteolytically resistant, and docosahexaenoic acid (DHA) treatment alleviated the stress responses in the AD neural cells. Differential manifestation of ER stress and DHA responsiveness may help explain variable clinical results obtained with the use of DHA treatment and suggests that DHA may in fact be effective for a subset of patients. It also illustrates how patient-specific iPSCs can be useful for analyzing AD pathogenesis and evaluating drugs.

INTRODUCTION

Alzheimer's disease (AD) is the most prevalent neurodegenerative disorder. One of the pathological features of AD is the oligomerization and aggregation and accumulation of amyloid-β peptide (Aβ), forming amyloid plaques in the brain. Cognitive impairment observed in clinical AD is inversely well correlated with the amount of Aβ oligomers in the soluble fraction rather than the amount of Aβ fibrils (amyloid plaques) constituting the oligomers (Haass and Selkoe, 2007; Krafft and Klein, 2010). Increasing evidence has shown that Aβ oligomers extracted from AD model mice or made from synthetic peptides cause

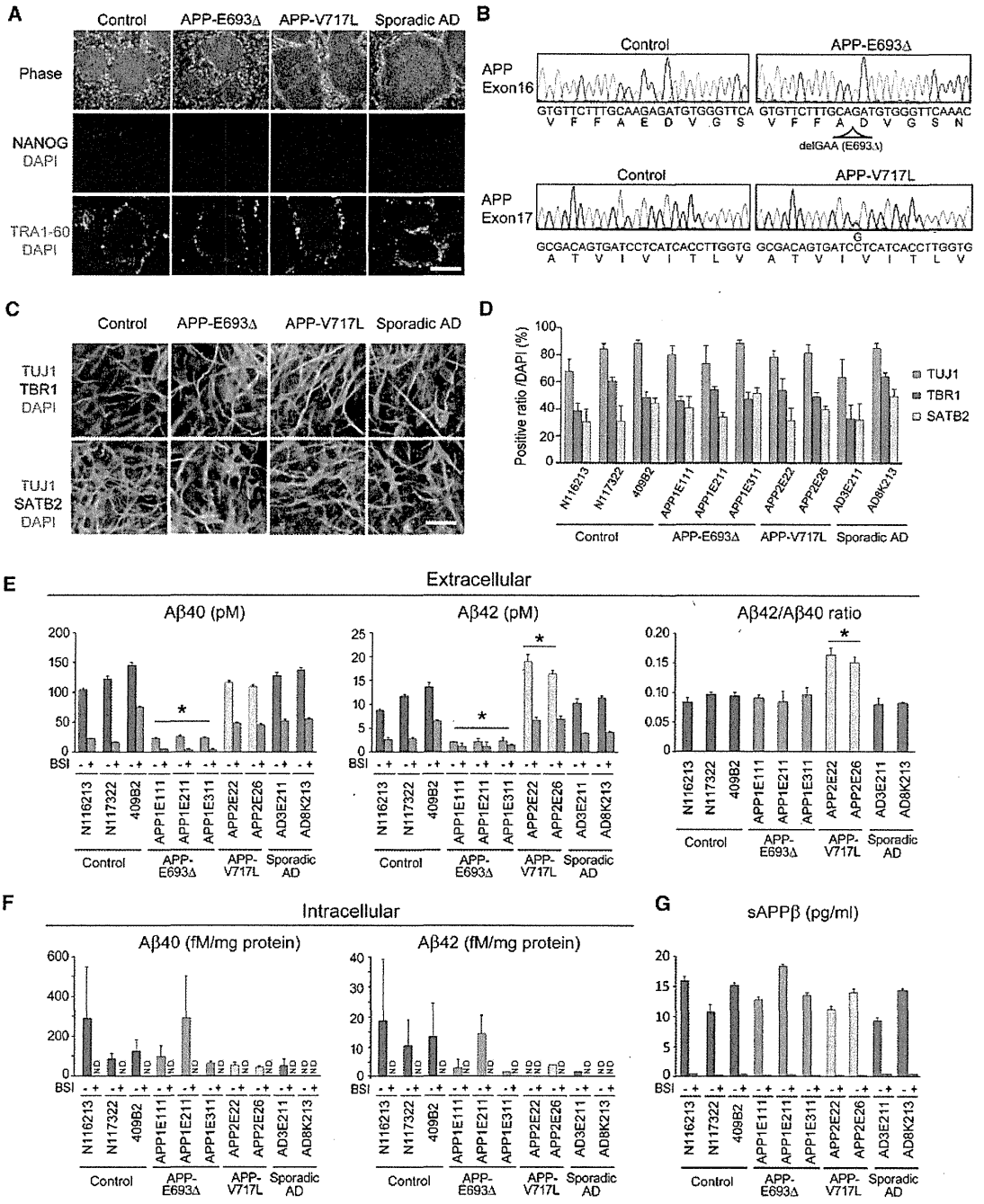

Figure 1. Establishment of Control and AD Patient-Specific iPSCs, and Derivation of Cortical Neurons Producing Aβs from iPSCs

(A) Established iPSCs from both controls and AD patients showed embryonic stem cell-like morphology (Phase) and expressed pluripotent stem cell markers NANOG (red) and TRA1-60 (green). The scale bar represents 200 μm.

(B) Genomic DNA sequences showed the presence of the homozygous genotype for E693 deletion and the heterozygous genotype for V717L mutation on the *APP* gene only in AD iPSCs.

(C) Estimation of neuronal differentiation from control and AD-iPSCs. After 2 months of differentiation, neurons were immunostained with antibodies against the neuronal marker TUJ1 and the cortical neuron markers TBR1 and SATB2. The scale bar represents 30 μm.

(D) Proportions of TUJ1-, TBR1-, and SATB2-positive cells in control and AD-iPSCs. Data represent mean ± SD ($n = 3$ per clone).

(E) Aβ40 and Aβ42 secreted from iPSC-derived neural cells into the medium (extracellular Aβ) were measured at 48 hr after the last medium change. Data represent mean ± SD ($n = 3$ per clone). Levels of Aβ40 and Aβ42 in AD(APP-E693Δ) without β-secretase inhibitor IV (BSI, 1 μM) were significantly lower than those of the others (*, $p < 0.006$), and the level of Aβ42 and the ratio of Aβ42/Aβ40 in AD(APP-V717L) without BSI were significantly higher than those of the others

(legend continued on next page)

neurotoxicity and cognitive impairments in vitro and in vivo (Walsh et al., 2002; Gong et al., 2003; Lesné et al., 2006), and this was also true in humans (Kuo et al., 1996; Shankar et al., 2008; Noguchi et al., 2009). Therefore, the formation and accumulation of Aβ oligomers has been presumed to play a central role in the pathogenesis and clinical symptoms of AD. Aβs are composed of 38–43 amino acid residues and are generated from the amyloid precursor protein (APP) by β- and γ-secretase-mediated sequential cleavages. A number of mutations linked to familial AD in the *APP* gene have been identified. Recently, an atypical early-onset familial AD, caused by an E693Δ mutation of an APP-producing variant Aβ lacking 22nd Glu was discovered in Japan (Tomiyama et al., 2008). This APP-E693Δ mutation presents rare, autosomal-recessive mutations of the *APP* gene related to familial AD. Patients with the mutation show overt early-onset symptoms of AD but lack Aβ deposition, according to positron emission tomography (PET) scan analysis with a [^{11}C] Pittsburgh compound-B (PIB) radioprobe (Tomiyama et al., 2008; Shimada et al., 2011). The 22nd Glu within the Aβ sequence has a destabilizing effect on the formation of oligomeric structures because of the electrostatic repulsion between the adjacent side chain of 22nd Glu (Kassler et al., 2010), and the deletion of the amino acid residue leads to the ready formation of Aβ oligomers in vitro (Nishitsuji et al., 2009). APP-E693Δ transgenic mice show AD-like pathology, including intracellular oligomer accumulation, but lack extracellular amyloid plaque formation (Tomiyama et al., 2010). However, it remains unclear whether Aβ oligomers are accumulated in familial and sporadic AD patient neural cells and how intracellular Aβ oligomers play a pathological role. The compound and/or drugs that might rescue the Aβ oligomer-induced pathological phenotypes are also unclear. Recent developments in induced pluripotent stem cell (iPSC) technology have facilitated the investigation of phenotypes of patient neural cells in vitro and have helped to overcome the lack of success in modeling sporadic AD.

Here, we report the derivation and neuronal and astroglial differentiation of iPSCs from a familial AD patient with an APP-E693Δ mutation, a familial case with another APP mutation, as well as other sporadic cases. Using patient neurons and astrocytes, we addressed the accumulation and possible pathological roles of intracellular Aβ oligomers in familial and sporadic AD. We found that Aβ oligomers were not proteolytically resistant and that docosahexaenoic acid (DHA) treatment attenuated cellular phenotypes of AD neural cells with intracellular Aβ oligomers in both familial and sporadic AD patients.

RESULTS

iPSC Generation and Cortical-Neuronal Differentiation

Dermal fibroblasts were reprogrammed by episomal vectors (Okita et al., 2011). Control iPSC lines from three unrelated individuals, three and two familial AD iPSC lines from patients with E693Δ[AD(APP-E693Δ)] and V717L[AD(APP-V717L)] APP mutations, respectively, and two sporadic iPSC lines (AD3E211 and AD8K213) from two unrelated patients (Figure S1A available online) were generated (Figures 1A, 1B, and S1B–S1H). To characterize cortical neurons derived from the iPSC lines, we established differentiation methods for cortical neurons by modifying previous procedures (Morizane et al., 2011) (Figure S1I). The differentiated cells expressed the cortical neuron subtype markers SATB2 and TBR1 (Figure 1C), and the differentiated neurons were functionally active (Figures S1J and S1K). There was no prominent difference in the differentiation propensity between control and AD neurons (Figures 1D and S1L).

We analyzed the amounts of extra- and intracellular Aβ40 and Aβ42 (Figures 1E and 1F). As expected, both Aβ species were strongly decreased in all cloned AD(APP-E693Δ) neural cells in comparison to those in control neural cells. In familial AD(APP-V717L) neural cells, an increase in the extracellular Aβ42 level and a corresponding decrease in the intracellular Aβ42 level were observed, and the Aβ42/Aβ40 ratio in the culture medium was increased up to 1.5-fold, suggesting that the abnormality of APP metabolism in AD is dependent on the mutation sites in *APP*. Extracellular Aβ levels in sporadic AD neural cells were not changed in comparison to those in control neural cells, but intracellular Aβ in sporadic AD8K213 neural cells apparently decreased (that is, below the detection limit). APP expression levels in the AD(APP-E693Δ) neural cells were lower than in the others, but the levels of α- and β-secretase-mediated APP processing remained unaltered in all neural cells (Figures 1G, S1M, and S1N). Soluble APPβ production was strongly inhibited by treatment with β-secretase inhibitor IV (BSI) (Figure 1G). Aβ levels in the original fibroblasts and iPSC-derived astrocytes, in which APP expression levels were relatively higher than those in neural cells (data not shown), were lower than those of the corresponding neural cells (Figures S1O and S1P).

Intracellular Accumulation of Aβ Oligomers in AD(APP-E693Δ) and in One of the Sporadic AD Neural Cells

Using an immunocytochemical method with the Aβ-oligomer-specific antibody NU1 (Lambert et al., 2007), we investigated whether AD(APP-E693Δ) neural cells harbor Aβ oligomers or not. We found that Aβ oligomers were accumulated as puncta in the neurons of AD(APP-E693Δ) and in one of the sporadic AD cases (Figure 2A). The area of Aβ-oligomer-positive puncta was significantly increased in AD(APP-E693Δ) neuronal cells relative to control neuronal cells (Figure 2B). Dot blot analysis using cell lysates revealed that Aβ oligomers were markedly elevated in the AD(APP-E693Δ) and sporadic AD8K213 neural cells (Figures 2C and 2D), whereas Aβ oligomers were not detected in the culture medium (data not shown). Another antibody against Aβ, 11A1, which detects low-molecular-weight oligomers rather than the Aβ monomer (Murakami et al., 2010), showed results similar to those observed with NU1 (Figures

(*, $p < 0.001$). There are significant differences between dimethyl sulfoxide (DMSO)-control and BSI treatment in each case (*, $p < 0.001$) except that of AD(APP-E693Δ) for Aβ42.

(F) Aβ40 and Aβ42 in cell lysates (intracellular Aβ). N.D., not detected. Data represent mean ± SD ($n = 3$ per clone).

(G) The amount of soluble APPβ was not altered in control and AD. Data represent mean ± SD ($n = 3$ per clone).

See also Figure S1.

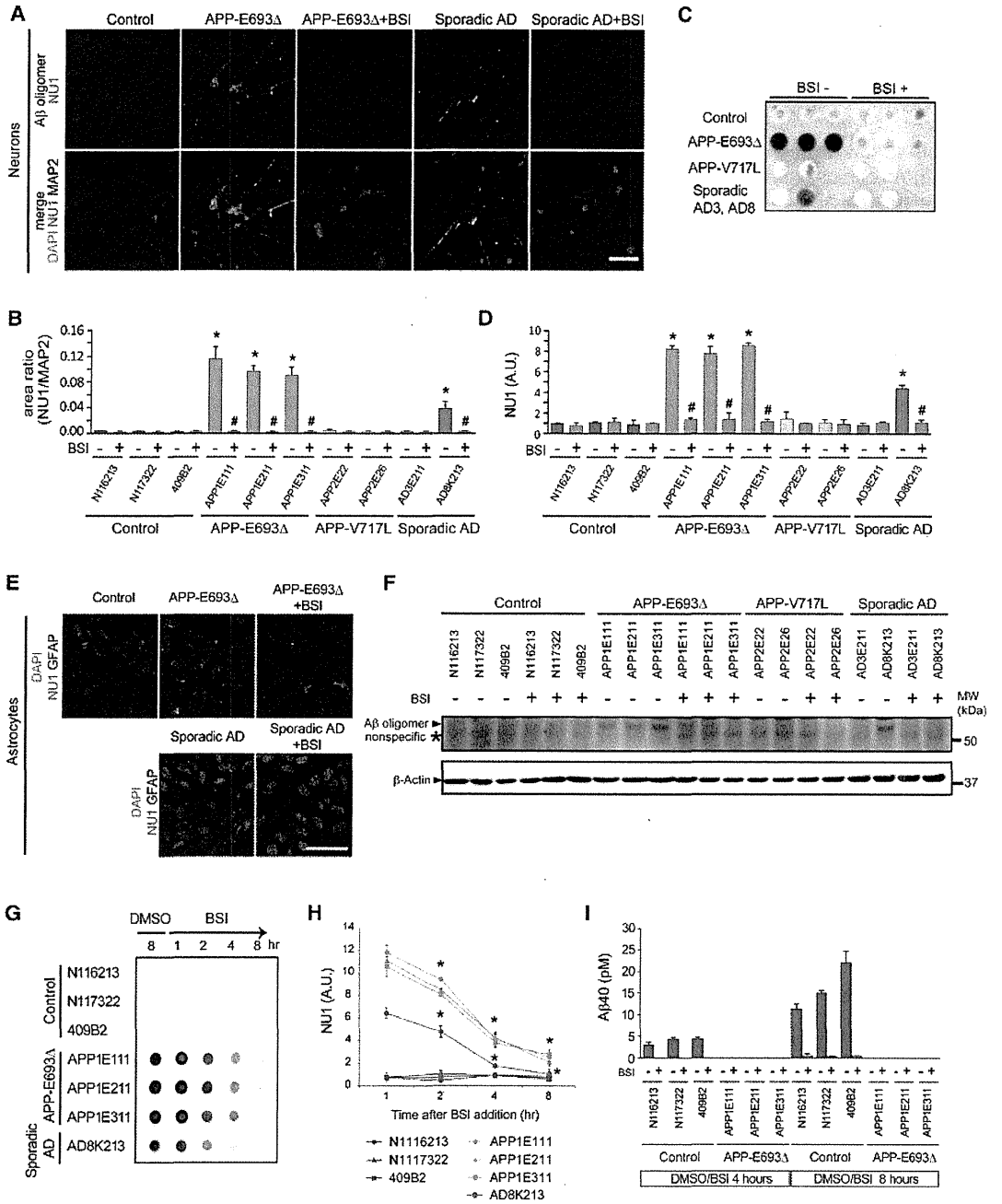

Figure 2. Familial AD(APP-E693Δ) and Sporadic AD iPSC-Derived Neurons Have Intracellular Aβ Oligomers

(A) Intracellular Aβ oligomer accumulation in iPSC-derived neurons (red, MAP2-positive cells) was detected by the Aβ-oligomer-specific monoclonal antibody NU1 (green) with a punctate pattern. Aβ oligomer accumulation was massive in AD(APP-E693Δ) and sporadic AD(AD8K213) neurons but only faint in control neurons. Treatment with 1 μM BSI decreased Aβ oligomer accumulation. DAPI, nuclear staining (blue). The scale bar represents 30 μm.

(B) Quantification of Aβ oligomer accumulation in (A); the ratio of the NU1-positive area in the MAP2-positive area was analyzed. Data represent mean ± SD (n = 3 per clone). Aβ oligomer levels in the AD(APP-E693Δ) and sporadic AD(AD8K213) neural cells without BSI were significantly different from those of other neural cells (*, $p < 0.005$) and from corresponding neural cells with BSI (#, $p < 0.005$).

(C) Dot blot analysis with the use of NU1 antibody. Control (N116213, N117322, 409B2), APP-E693Δ(APP1E111, APP1E211, APP1E211), APP-V717L (APP2E22, APP2E26), and sporadic AD (AD3E211, AD8K213) neural cells were dotted from the left. Blank is RIPA buffer only.

(D) Signals of blot in (C) were quantified. Data represent mean ± SD (n = 3 per clone). Aβ oligomer levels in AD(APP-E693Δ) and sporadic AD(AD8K213) neurons without BSI were significantly different from those of other neurons (*, $p < 0.001$) and from corresponding neurons treated with 1 μM BSI (#, $p < 0.001$).

(E) Aβ oligomer accumulation in AD astrocytes. The scale bar represents 30 μm.

(legend continued on next page)

S2A–S2D). However, Aβ oligomers were not detected in cell lysates from the fibroblasts that generate iPSC lines (Figure S2E). To confirm whether Aβ oligomers were derived from mutant APP(E693Δ), we transduced a lentiviral vector driven by an EF1α promoter to overexpress wild or mutant APP(E693Δ) in control iPSC-derived neural cells and found that Aβ oligomers emerged inside control neural cells overexpressing mutant APP(E693Δ) (Figure S2F).

To investigate the intracellular accumulation of Aβ oligomers in astrocytes derived from control and AD iPSCs, we established an astrocyte-enrichment culture by modifying the method previously reported (Krencik et al., 2011) (Figures S2G–S2J). Dot blot analysis using Aβ oligomer antibodies revealed that the astrocytes of AD(APP-E693Δ) and one of the sporadic AD iPSCs accumulated Aβ oligomers intracellularly (Figures 2E, S2K, and S2L), which was compatible with the results of neurons. On the other hand, we detected no difference in the uptake of extracellular glutamate between control and AD astrocytes (Figure S2M).

Aβ oligomers were also detected as a protein band with a molecular mass of 50□60 kDa by western blot analysis (Figures 2F and S2N). The accumulation of Aβ oligomers was inhibited by treatment with BSI (Figures 2A–2G, S2A–S2D, and S2N). To clarify whether the E693Δ mutation results in accelerated Aβ oligomerization and/or in a proteolytically resistant and stable form of Aβ oligomers, we analyzed the levels of Aβ oligomers over a course of time after BSI treatment. Intracellular Aβ oligomers started to disappear from 2 hr after the treatment with BSI, almost reaching the control level by 8 hr (Figures 2G and 2H). Secretion of Aβ40 from control neural cells was already inhibited at 2 hr after BSI treatment, but the secretion from AD neural cells was under the detection limit in both the presence and absence of BSI (Figure 2I).

Cellular Stress Responses Caused By Intracellular Aβ Oligomers in AD iPSC-Derived Neural Cells

Extracellular Aβ deposition in patient brains carrying APP with an E693Δ mutation is predicted to be extremely low, as amyloid PET imaging with a [^{11}C] PIB probe revealed a far lower signal in the patients than those observed in sporadic AD brains (Tomiyama et al., 2008). Given that processing by β- and γ-secretases largely proceeds within vesicular endosomal compartments, it was possible that Aβ oligomers were associated with specific organelles. We characterized the Aβ oligomer-positive punctate structures in AD(APP-E693Δ) neural cells and astrocytes by coimmunostaining with antibodies for markers of vesicular compartments and subcellular organelles. Subpopulations of Aβ oligomer-positive puncta in the AD neurons showed positive immunostaining for an endoplasmic reticulum (ER) marker, binding immunoglobulin protein (BiP); an early endosomal marker, early endosome-associated antigen-1 (EEA1); and a lysosomal marker, lysosomal-associated marker protein 2 (LAMP2) (data not shown).

To uncover molecules that might be implicated in the dysfunction of AD(APP-E693Δ) neural cells, we analyzed gene expression profiles of control and AD neural cells (Figure 3A and Table S1). Gene ontology analysis revealed that oxidative-stress-related categories, including peroxiredoxin, oxidoreductase, and peroxidase activities, were upregulated in the AD, whereas glycosylation-related categories were downregulated (Figures 3B and 3C and Table S1), suggesting that ER and Golgi function might be perturbed in AD neural cells. Western blot analysis clarified that the amounts of both BiP and cleaved caspase-4 were elevated in the neurons and astrocytes of the AD(APP-E693Δ) case, and that of BiP in one of the sporadic AD cases, AD8K213, but not in fibroblasts (Figures 3D–3F and S3A–S3F). We also found that BSI treatment not only prevented the increase in Aβ oligomer-positive puncta area per cell in the context of AD(APP-E693Δ) lines but also decreased the amount of BiP and cleaved caspase-4 (Figures 3D–3F). *PRDX4*-coding antioxidant protein peroxiredoxin-4 was the most highly upregulated gene (Figure 3C). Western blot analysis confirmed that the amount of peroxiredoxin-4 was increased up to approximately 5- to 7-fold in lysates from AD(APP-E693Δ) and in one of the sporadic AD cases, AD8K213 neural cells, but not in fibroblasts, and was decreased by the BSI treatment (Figures 3D, 3G, S3A, S3D, S3G, and S3H), indicating that the antioxidant stress response was provoked by Aβ oligomer formation in AD(APP-E693Δ) and sporadic AD8K213. To identify pathogenic species evoking oxidative stress in AD(APP-E693Δ), we visualized reactive oxygen species (ROS) and found that ROS was increased in both neurons and astrocytes in AD(APP-E693Δ) and AD8K213 (Figures 3H–3J and S3I –S3L). This increase was counteracted by the BSI treatment. These results indicated that intracellular Aβ oligomers provoked both ER and oxidative stress, and the increase in ROS most likely occurred via a vicious cycle between ER and oxidative stress (Malhotra and Kaufman, 2007).

Alleviation of Intracellular Aβ Oligomer-Induced Cellular Stress by DHA

We evaluated BSI and three additional drugs that had been reported to improve ER stress or to inhibit ROS generation: (1) DHA (Begum et al., 2012), (2) dibenzoylmethane (DBM14-26) (Takano et al., 2007), and (3) NSC23766 (Lee et al., 2002) (Figures 4 and S4). DHA treatment significantly decreased the protein level of BiP, cleaved caspase-4, and peroxiredoxin-4 in AD (APP-E693Δ) neural cells (Figures 4A, 4B, S4A, and S4B), and BiP and peroxiredoxin-4 in sporadic AD8K213 (Figures S4C and S4D). Furthermore, DHA treatment also decreased the generation of ROS in AD(APP-E693Δ) neural cells (Figures 4C and 4D), whereas the amount of Aβ oligomers in cell lysates

(F) Western blot analysis of control and AD neural cells in the presence or absence of BSI. BSI treatment (1 μM) disappeared 6E10-positive ≥ 55 kDa protein bands in cell lysates of AD(APP-E693Δ) and sporadic AD(AD8K213) neural cells.

(G) Disappearance of Aβ oligomers after BSI treatment was analyzed by dot blot analysis with the use of the NU1 antibody. Intracellular Aβ oligomers started to disappear 2 hr after BSI treatment.

(H) Signals of blots in (G) were quantified. Data represent mean ± SD (n = 3 per clone). BSI treatment (1 μM) decreased intracellular Aβ in AD neural cells and was reduced to 16□23% of vehicle control by 8 hr. Post hoc analysis revealed that the amounts of Aβ oligomers at 2 hr after BSI treatment were significantly decreased in comparison to those of DMSO control oligomers (*, $p < 0.005$).

(I) Changes in extracellular Aβ40 levels were analyzed in the experimental condition of (G). Data represent mean ± SD (n = 3 per clone).

See also Figure S2.

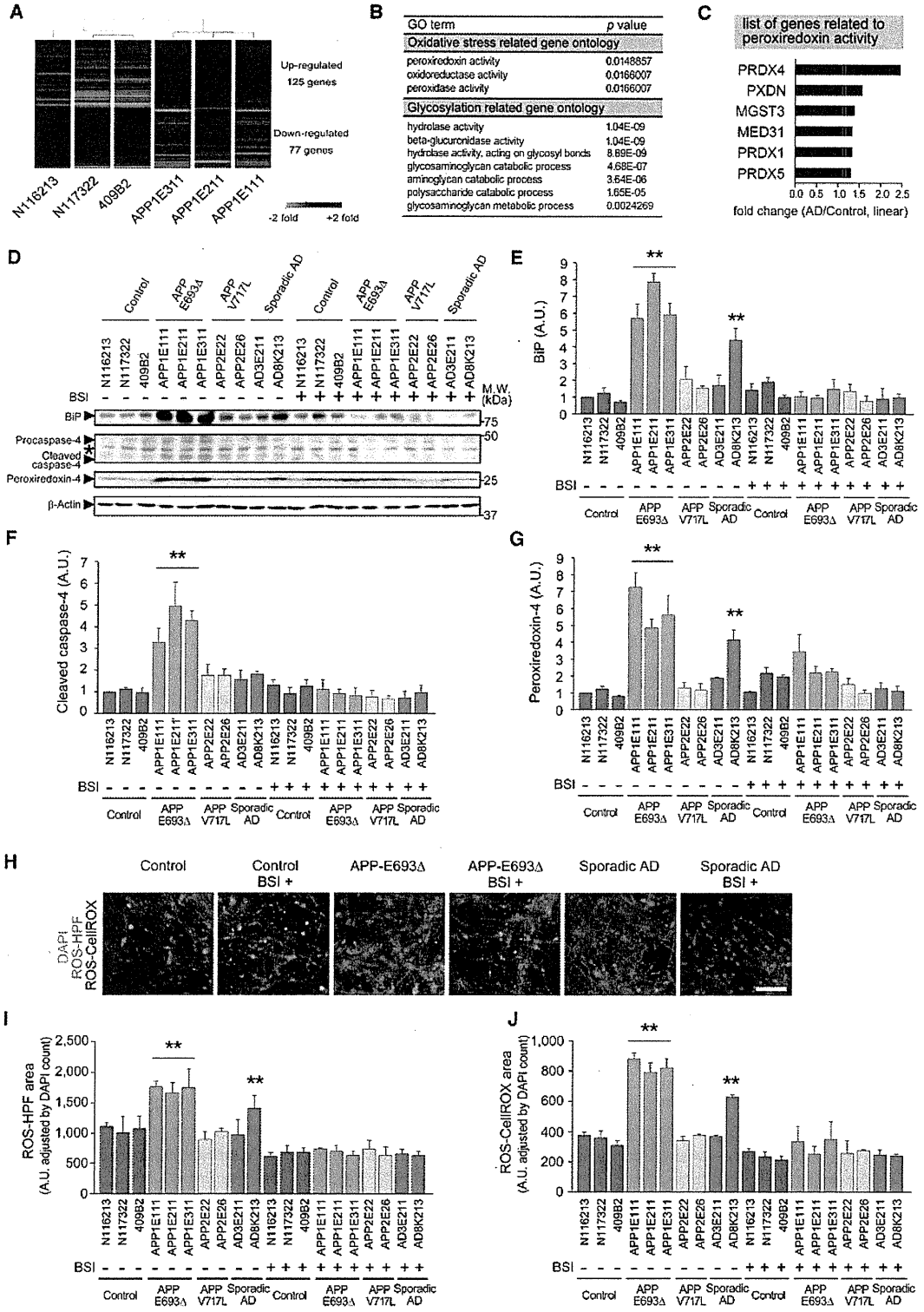

Figure 3. Cellular Stress Responses Caused by Intracellular Aβ Oligomers in Familial AD(APP-E693Δ) and Sporadic AD(AD8K213) iPSC-Derived Neural Cells

(A) Hierarchical clustering analysis of differentiated neuronal cells and a heatmap of significantly up- and downregulated genes in AD neural cells. The statistically significant cutoff p value is < 0.05.

(legend continued on next page)

was not altered (Figures S4E–S4G). In contrast, the high concentration of DHA, DBM14-26, or NSC23766 treatment increased the protein level of BiP (Figure S4B). Finally, to confirm the protective effects of DHA in short-term screening, we analyzed the effect on the survival of AD(APP-E693Δ) neural cells. Neuronal cells were labeled with a lentiviral vector expressing synapsin I-promoter-driven EGFP and cultivated in the medium depleted of neurotrophic factors and neural culture supplements mix. The real-time survival rate of AD(APP-E693Δ) neurons was lower than that of normal control neurons; however, DHA treatment for 16 days partially rescued AD(APP-E693Δ) cell viability (Figures 4E–4G). The real-time survival rate of sporadic AD(AD3E211, AD8K213) neurons for 16 days was unchanged (Figures 4E and 4F and Table S2). We confirmed these results through a lactate dehydrogenase (LDH) assay (Figure 4G). The AD(APP-E693Δ) neurons were also vulnerable to oxidative stress by hydrogen peroxide treatment (Figure S4H). Extracellular Aβ levels were not altered in the assay (Figure 4H).

DISCUSSION

The present study shows that neural cells derived from a patient carrying the pathogenic APP-E693Δ mutation and a sporadic AD patient produce intracellular Aβ oligomers, and the use of these neural cells provided an experimental system for addressing whether such oligomers would cause cellular stress and the killing of neurons and how such intracellular Aβ oligomers might contribute to the disease pathogenesis, despite only one patient carrying the E693Δ mutation being available. Our findings also suggest that the possible heterogeneity of familial and sporadic AD stems from phenotypic differences of intracellular Aβ oligomers and suggests the possibility that DHA, a drug that failed in some clinical trials of AD treatment, might be effective in a portion of AD patients.

We demonstrated that Aβ oligomers were formed and accumulated inside AD(APP-E693Δ) and sporadic AD(AD8K213) neurons by immunostaining (Figures 2A and 2B), dot blot analysis (Figures 2C and 2D), and western blot analysis (Figures 2F and S2N). In addition, intracellular accumulation of Aβ oligomers, which has been supposed to be proteolytically resistant, disappeared after treatment with BSI in both AD neurons (Figures 2G and 2H), indicating that AD(APP-E693Δ) and sporadic AD(AD8K213) neurons still seemed to retain a degrading activity toward Aβ oligomers in which proteasomes, autophagosomes, and/or lysosomes may be involved and, thereby, that the pathological property of Aβ oligomers in a part of AD might be completely abrogated. The sporadic AD(AD8K213) neurons may retain a specific cellular environment that permits the formation of Aβ oligomers. Additional studies aimed at identifying the factors causing such an environment are needed.

We observed that the accumulation of Aβ oligomers induced ER and oxidative stress both in AD(APP-E693Δ) and in sporadic AD(AD8K213) neurons, although caspase-4 activation appeared not to accompany sporadic AD, probably because of the lesser extent of ER stress in comparison to AD(APP-E693Δ). Previously, Nishitsuji et al. (2009) reported that accumulated Aβ oligomers in ER provoke ER stress. This result suggests that oligomers represent a self-aggregating state of Aβ. During this process, Aβ generates ROS, which is supported by the fact that Aβ coordinates the metal ions zinc, iron, and copper, which induce the oligomerization of Aβ. Iron and copper then cause the generation of toxic ROS and calcium dysregulation (Barnham et al., 2004), leading to membrane lipid peroxidation and the impairment of the function of a range of membrane-associated proteins (Hensley et al., 1994; Butterfield, 2003), antioxidant factors being thought to protect ER-stress-induced cellular toxicities (Malhotra and Kaufman, 2007).

We found that intracellular Aβ oligomers were accumulated not only in a case of familial AD with APP-E693Δ mutation but also in a sporadic AD case, although only three clones derived from one familial AD patient carrying an APP-E693Δ mutation and two clones from two sporadic AD patients were analyzed in this study because of the limited number of patients. In contrast, in familial AD with the APP-V717L mutation, of which only one case was available, intracellular Aβ oligomers were not detected, but the extracellular Aβ42/Aβ40 ratio, which is increased in mutant presenilin-mediated familial AD, as reported previously (Yagi et al., 2011), was increased, lending support to the notion that AD could be classified into two categories: extracellular Aβ type and intracellular Aβ type. Although it has been supposed that environmental factors and/or the aging process contribute to neurodegenerative diseases, our findings support the idea that a genetic factor might play a role in a part of sporadic AD, a finding that is compatible with a previous report (Israel et al., 2012). However, identifying the genetic factor would require a larger sample size. The sporadic AD case with intracellular Aβ oligomers might correspond to the case without extracellular Aβ40 elevation of Israel et al. (2012). Analysis of neurons

(B) The gene ontology (GO) term list, calculated from the significantly altered gene expression patterns in the microarray analysis of AD versus control neural cells.
(C) Altered expression levels of genes related to peroxidation activity detected by GO analysis. All values were significantly different from that of the control ($p < 0.05$).
(D–G) Western blot analysis of ER stress markers (BiP and casapase-4), peroxiredoxin-4, and a reference protein (β-actin) in the presence or absence of BSI. (E–G) Densitometric analysis of (D) are shown. Measured values of proteins were normalized by β-actin. Data represent mean ± SD (n = 3 per clone). Levels of BiP (E), cleaved caspase-4 (F), and peroxiredoxin-4 (G) in AD(APP-E693Δ) and sporadic AD(AD8K213) neural cells without BSI were significantly different from those of the other neural cells (**, $p < 0.005$).
(H) Typical images of reactive oxygen species (ROS) staining, detected by HPF or CellROX, in control and AD neural cells with or without BSI treatment. Scale bars represent 30 μm.
(I and J) Quantitative data of (H), ROS-HPF (I), and ROS-CellROX (J). Each value was shown as a ratio of the HPF-stained or CellROX area (average of random 25 fields per sample) adjusted with DAPI counts. Data represent mean ± SD (n = 3 per clone). ROS-generation levels in AD(APP-E693Δ) and sporadic AD(AD8K213) neural cells were significantly different from those of the others (**, $p < 0.001$). Data represent mean ± SD (n = 3 per clone).
See also Figure S3 and Table S1.

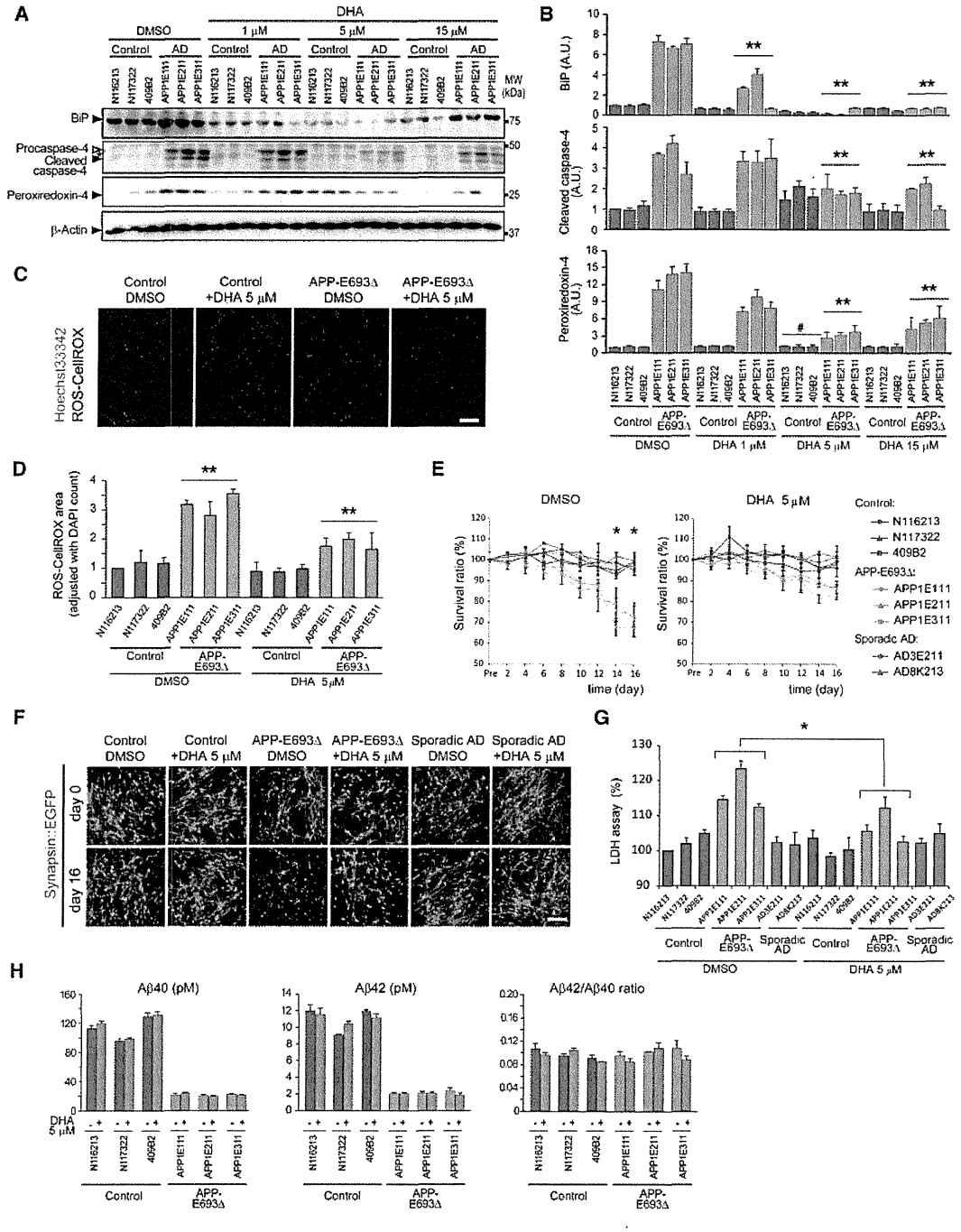

Figure 4. DHA-Alleviated Cellular Stress Caused By Intracellular Aβ Oligomers

(A) Control and AD(APP-E693Δ) neural cells at day 72 were treated with DHA for 48 hr. Then, cells were lysed and subjected to immunoblot analysis (1 μM, 5 μM, and 15 μM of docosahexaenoic acid [DHA]).

(B) Densitometric analysis of (A) is shown. Measured values were normalized by that of β-actin. Data represent mean ± SD (n = 3 per clone). Two-way analysis of variance (ANOVA) showed significant main effects of DHA treatment (BIP, $F_{[3,64]} = 136.712$, $p < 0.001$; cleaved caspase-4, $F_{[3,64]} = 50.855$, $p < 0.001$) with a significant interaction between APP mutation and DHA treatment (BIP, $F_{[3,64]} = 99.658$, $p < 0.001$; cleaved caspase-4, $F_{[3,64]} = 53.005$, $p < 0.001$). Post hoc analysis revealed significant differences between DMSO (control) and DHA treatment (1, 5, and 15 μM) in AD(APP-E693Δ) neural cells (**, $p < 0.001$). Two-way ANOVA for peroxiredoxin-4 showed significant main effects of DHA treatment ($F_{[3,64]} = 16.995$; $p < 0.001$) with a significant interaction between APP mutation and DHA treatment ($F_{[3,64]} = 32.093$; $p < 0.001$). Post hoc analysis revealed significant differences between DMSO-control and DHA treatment (5 and 15 μM) in AD(APP-E693Δ) neural cells (**, $p < 0.001$). In control neural cells, the 5 μM DHA group was significantly different from the other groups (#, $p < 0.005$).

(C) Typical images of ROS-CellROX and Hoechst33342 signals after treatment with vehicle or 5 μM DHA. The scale bar represents 50 μm.

(legend continued on next page)

and astrocytes, as we performed here, from larger numbers of patients might result in the classification of sporadic AD.

To date, the clinical effectiveness of DHA treatment is still controversial (Freund-Levi et al., 2006; Quinn et al., 2010). It is of particular interest that one of two sporadic AD neurons accumulated intracellular Aβ oligomers and showed cellular phenotypes that could respond to DHA but the other did not, and this result may explain why DHA treatment was effective for some AD patients, those with the intracellular Aβ oligomer-associated type of AD, although the timing (that is, the stage of disease development) for starting the treatment would be another critical factor. These results may suggest that patient-specific iPSCs provide a chance to re-evaluate the effect of a drug that failed in AD clinical trials, depending on the selection of the patient type. In the present study, the amount of Aβ oligomers in our culture was not affected by DHA, although it would be effective for reducing cellular stresses, and reducing the oligomerization of Aβ was also presumed to be a candidate mechanism of DHA treatment (Cole and Frautschy, 2006). These results indicate that therapy with DHA would alleviate symptoms. Furthermore, the data showing that BSI treatment leads to a reduction in ROS formation at a relatively similar level (Figure 2G) in both AD and control cells might indicate an Aβ oligomer-independent effect, in addition to an Aβ oligomer-dependent effect, of BSI.

In any event, patient-specific iPSCs would provide disease pathogenesis, irrespective of the disease being in a familial or sporadic form, as well as enable the evaluation of drug and patient classification of AD.

EXPERIMENTAL PROCEDURES

Derivation of Patient-Specific Fibroblasts

Control and AD-derived human dermal fibroblasts (HDFs) were generated from explants of 3 mm dermal biopsies. After 1–2 weeks, fibroblast outgrowths from the explants were passaged.

iPSC Generation

Human complementary DNAs for reprogramming factors were transduced in HDFs with episomal vectors (*SOX2, KLF4, OCT4, L-MYC, LIN28*, and small hairpin RNA for p53). Several days after transduction, fibroblasts were harvested and replated on an SNL feeder cell layer. On the following day, the medium was changed to a primate embryonic stem cell medium (ReproCELL, Japan) supplemented with 4 ng/ml basic FGF (Wako Pure Chemicals Industries, Japan). The medium was changed every other day. iPSC colonies were picked up 30 days after transduction.

Statistical Analysis

All data are shown as mean ± SD. For comparisons of the mean between two groups, statistical analysis was performed by applying Student's t tests after confirming equality between the variances of the groups. When the variances were unequal, Mann-Whitney U tests were performed (SigmaPlot 11.2.0, Systat Software, USA). Comparisons of the mean among three groups or more were performed by one-way, two-way, or three-way analysis of variance followed by a post hoc test with the use of Student-Newman-Keuls Method (SigmaPlot 11.2.0). p values < 0.05 were considered significant.

ACCESSION NUMBERS

The Gene Expression Omnibus accession numbers for microarray data reported in this paper are GSE43326 (gene-expression comparison between control and AD clones), GSE43382 (gene-expression change along with the astroglial differentiation), and GSE43328 (gene-expression comparison of generated iPSCs).

SUPPLEMENTAL INFORMATION

Supplemental Information contains Supplemental Experimental Procedures, four figures, and two tables and can be found with this article online at http://dx.doi.org/10.1016/j.stem.2013.01.009.

ACKNOWLEDGMENTS

We would like to express our sincere gratitude to all our coworkers and collaborators, Mari Ohnuki, Megumi Kumazaki, Mitsuyo Kawada, Fumihiko Adachi, Takako Enami, and Misato Funayama for technical assistance; Nobuya Inagaki and Norio Harada for technical advice; and Kazumi Murai for editing the manuscript. This research was funded in part by a grant from the Funding Program for World-Leading Innovative R&D on Science and Technology (FIRST Program) of the Japan Society for the Promotion of Science (JSPS) to S.Y., from the Alzheimer's Association (IIRG-09-132098) to H.M., from the JST Yamanaka iPS Cell Special Project to S.Y. and H.I., from CREST to H.I., H.M., N.I., and T.T., from a Grant-in-Aid from the Ministry of Health, Labour and Welfare of Japan to H.I., from a Grant-in-Aid for Scientific Research on Innovative Area "Foundation of Synapse and Neurocircuit Pathology" (22110007) from the Ministry of Education, Culture, Sports, Science and Technology of Japan to H.I. and N.I., and from the Japan Research Foundation for Clinical Pharmacology to H.I. H.I. conceived the project; T.K., N.I., M.A., and H.I. designed the experiments; T.K., N.I., M.A., K.W., C.K., R.N., N.E., N.Y. and K. Tsukita performed the experiments; T.K., N.I., M.A., and H.I. analyzed the data; K.O., I.A., K.M., T.N., K.I., W.L.K., O.H., S.H., and T.C. contributed

(D) Quantitative data of (C) is shown. Each value indicated the ratio of the CellROX-stained area (an average of random 25 fields per sample) adjusted with DAPI counts. Data represent mean ± SD (n = 3 per clone). Two-way ANOVA showed significant main effects of DHA treatment ($F_{[1,32]} = 43.140$; $p < 0.001$) with a significant interaction between the APP mutation and DHA treatment ($F_{[3,32]} = 23.410$; $p < 0.001$). The DHA group in AD(APP-E693Δ) neural cells was significantly different from the other groups (**, $p < 0.005$).

(E) Real-time survival rate of control and AD neural cells with and without DHA showing cell viability. The numbers of control and AD(APP-E693Δ) neurons with Synapsin I-promoter-driven EGFP were sequentially imaged (average of 25 random fields per sample) and counted to assess the survival ratio (n = 3 per clone). Data represent mean ± SD (n = 3 per clone). In the cell-survival ratio, three-way ANOVA showed significant main effects of the APP mutation ($F_{[1,256]} = 377.611$; $p < 0.001$), DHA treatment ($F_{[1,256]} = 36.117$; $p < 0.001$), and time ($F_{[7,256]} = 65.272$; $p < 0.001$), with significant interactions between the APP mutation and DHA treatment ($F_{[1,256]} = 18.315$; $p < 0.001$), between the APP mutation and time ($F_{[7,256]} = 20.023$; $p < 0.001$), between DHA treatment and time ($F_{[7,256]} = 4.534$; $p < 0.001$), and among all three factors ($F_{[7,256]} = 5.277$; $p < 0.001$). Post hoc analysis revealed that, on day 14 and day 16, AD(APP-E693Δ) neural cells were more vulnerable in the long culture than control neural cells and that DHA treatment rescued the vulnerability (*, $p < 0.001$).

(F) Typical images of Synapsin::EGFP neurons used in real-time survival assay. The scale bar represents 50 μm.

(G) Cytotoxicity in neural culture derived from control and AD iPSCs after treatment with DHA (5 μM) for 16 days. Measured fluorescent lactate dehydrogenase (LDH) release served as a measure of cytotoxicity. Data represent mean ± SD (n = 3 per clone). Two-way ANOVA showed significant main effects of DHA treatment ($F_{[1,32]} = 16.710$; $p < 0.001$) with a significant interaction between APP-E693Δ mutation and DHA treatment ($F_{[3,32]} = 9.210$; $p < 0.005$). There was a significant difference in AD(APP-E693Δ) neural cells between the DMSO-control and DHA groups (*, $p < 0.05$).

(H) Aβ40 and Aβ42 secreted from iPSC-derived neurons into medium (extracellular Aβ) at day 16 of the long-term culture were measured at 48 hr after the last medium change. Data represent mean ± SD (n = 3 per clone).

See also Figure S4 and Table S2.

reagents, materials and analysis tools; Y.K., Y.O., Y.S., M.N., K.Y., S.Y., S.S., T.A., R.H., and S.U. recruited the patients; R.T., H.M., and S.Y. provided critical reading and scientific discussions; T.S., K.K., T.T., and K. Takahashi performed microarray analysis; T.A. performed karyotyping; A.W. performed bisulfite genomic sequencing; K.I. and D.W. performed electrophysiology; K. Tsukita, T.K., and H.H. produced the lentivirus; H.I., N.I., M.A., and T.K. wrote the paper. The experimental protocols dealing with human or animal subjects were approved by the institutional review board at each institute. S.Y. is a member without salary of the scientific advisory boards of iPierian, iPS Academia Japan, Megakaryon Corporation, and Retina Institute Japan.

Received: February 27, 2012
Revised: December 22, 2012
Accepted: January 18, 2013
Published: February 21, 2013

REFERENCES

Barnham, K.J., Masters, C.L., and Bush, A.I. (2004). Neurodegenerative diseases and oxidative stress. Nat. Rev. Drug Discov. *3*, 205–214.

Begum, G., Kintner, D., Liu, Y., Cramer, S.W., and Sun, D. (2012). DHA inhibits ER Ca^{2+} release and ER stress in astrocytes following in vitro ischemia. J. Neurochem. *120*, 622–630.

Butterfield, D.A. (2003). Amyloid β-peptide [1-42]-associated free radical-induced oxidative stress and neurodegeneration in Alzheimer's disease brain: mechanisms and consequences. Curr. Med. Chem. *10*, 2651–2659.

Cole, G.M., and Frautschy, S.A. (2006). Docosahexaenoic acid protects from amyloid and dendritic pathology in an Alzheimer's disease mouse model. Nutr. Health *18*, 249–259.

Freund-Levi, Y., Eriksdotter-Jönhagen, M., Cederholm, T., Basun, H., Faxén-Irving, G., Garlind, A., Vedin, I., Vessby, B., Wahlund, L.O., and Palmblad, J. (2006). Omega-3 fatty acid treatment in 174 patients with mild to moderate Alzheimer disease: OmegAD study: a randomized double-blind trial. Arch. Neurol. *63*, 1402–1408.

Gong, Y., Chang, L., Viola, K.L., Lacor, P.N., Lambert, M.P., Finch, C.E., Krafft, G.A., and Klein, W.L. (2003). Alzheimer's disease-affected brain: presence of oligomeric A β ligands (ADDLs) suggests a molecular basis for reversible memory loss. Proc. Natl. Acad. Sci. USA *100*, 10417–10422.

Haass, C., and Selkoe, D.J. (2007). Soluble protein oligomers in neurodegeneration: lessons from the Alzheimer's amyloid β-peptide. Nat. Rev. Mol. Cell Biol. *8*, 101–112.

Hensley, K., Carney, J.M., Mattson, M.P., Aksenova, M., Harris, M., Wu, J.F., Floyd, R.A., and Butterfield, D.A. (1994). A model for β-amyloid aggregation and neurotoxicity based on free radical generation by the peptide: relevance to Alzheimer disease. Proc. Natl. Acad. Sci. USA *91*, 3270–3274.

Israel, M.A., Yuan, S.H., Bardy, C., Reyna, S.M., Mu, Y., Herrera, C., Hefferan, M.P., Van Gorp, S., Nazor, K.L., Boscolo, F.S., et al. (2012). Probing sporadic and familial Alzheimer's disease using induced pluripotent stem cells. Nature *482*, 216–220.

Kassler, K., Horn, A.H., and Sticht, H. (2010). Effect of pathogenic mutations on the structure and dynamics of Alzheimer's A β 42-amyloid oligomers. J. Mol. Model. *16*, 1011–1020.

Krafft, G.A., and Klein, W.L. (2010). ADDLs and the signaling web that leads to Alzheimer's disease. Neuropharmacology *59*, 230–242.

Krencik, R., Weick, J.P., Liu, Y., Zhang, Z.J., and Zhang, S.C. (2011). Specification of transplantable astroglial subtypes from human pluripotent stem cells. Nat. Biotechnol. *29*, 528–534.

Kuo, Y.M., Emmerling, M.R., Vigo-Pelfrey, C., Kasunic, T.C., Kirkpatrick, J.B., Murdoch, G.H., Ball, M.J., and Roher, A.E. (1996). Water-soluble Abeta (N-40, N-42) oligomers in normal and Alzheimer disease brains. J. Biol. Chem. *271*, 4077–4081.

Lambert, M.P., Velasco, P.T., Chang, L., Viola, K.L., Fernandez, S., Lacor, P.N., Khuon, D., Gong, Y., Bigio, E.H., Shaw, P., et al. (2007). Monoclonal antibodies that target pathological assemblies of Abeta. J. Neurochem. *100*, 23–35.

Lee, M., You, H.J., Cho, S.H., Woo, C.H., Yoo, M.H., Joe, E.H., and Kim, J.H. (2002). Implication of the small GTPase Rac1 in the generation of reactive oxygen species in response to β-amyloid in C6 astroglioma cells. Biochem. J. *366*, 937–943.

Lesné, S., Koh, M.T., Kotilinek, L., Kayed, R., Glabe, C.G., Yang, A., Gallagher, M., and Ashe, K.H. (2006). A specific amyloid-β protein assembly in the brain impairs memory. Nature *440*, 352–357.

Malhotra, J.D., and Kaufman, R.J. (2007). Endoplasmic reticulum stress and oxidative stress: a vicious cycle or a double-edged sword? Antioxid. Redox Signal. *9*, 2277–2293.

Morizane, A., Doi, D., Kikuchi, T., Nishimura, K., and Takahashi, J. (2011). Small-molecule inhibitors of bone morphogenic protein and activin/nodal signals promote highly efficient neural induction from human pluripotent stem cells. J. Neurosci. Res. *89*, 117–126.

Murakami, K., Horikoshi-Sakuraba, Y., Murata, N., Noda, Y., Masuda, Y., Kinoshita, N., Hatsuta, H., Murayama, S., Shirasawa, T., Shimizu, T., and Irie, K. (2010). Monoclonal antibody against the turn of the 42-residue amyloid β-protein at positions 22 and 23. ACS Chem. Neurosci. *1*, 747–756.

Nishitsuji, K., Tomiyama, T., Ishibashi, K., Ito, K., Teraoka, R., Lambert, M.P., Klein, W.L., and Mori, H. (2009). The E693Δ mutation in amyloid precursor protein increases intracellular accumulation of amyloid β oligomers and causes endoplasmic reticulum stress-induced apoptosis in cultured cells. Am. J. Pathol. *174*, 957–969.

Noguchi, A., Matsumura, S., Dezawa, M., Tada, M., Yanazawa, M., Ito, A., Akioka, M., Kikuchi, S., Sato, M., Ideno, S., et al. (2009). Isolation and characterization of patient-derived, toxic, high mass amyloid β-protein (Abeta) assembly from Alzheimer disease brains. J. Biol. Chem. *284*, 32895–32905.

Okita, K., Matsumura, Y., Sato, Y., Okada, A., Morizane, A., Okamoto, S., Hong, H., Nakagawa, M., Tanabe, K., Tezuka, K., et al. (2011). A more efficient method to generate integration-free human iPS cells. Nat. Methods *8*, 409–412.

Quinn, J.F., Raman, R., Thomas, R.G., Yurko-Mauro, K., Nelson, E.B., Van Dyck, C., Galvin, J.E., Emond, J., Jack, C.R., Jr., Weiner, M., et al. (2010). Docosahexaenoic acid supplementation and cognitive decline in Alzheimer disease: a randomized trial. JAMA *304*, 1903–1911.

Shankar, G.M., Li, S., Mehta, T.H., Garcia-Munoz, A., Shepardson, N.E., Smith, I., Brett, F.M., Farrell, M.A., Rowan, M.J., Lemere, C.A., et al. (2008). Amyloid-β protein dimers isolated directly from Alzheimer's brains impair synaptic plasticity and memory. Nat. Med. *14*, 837–842.

Shimada, H., Ataka, S., Tomiyama, T., Takechi, H., Mori, H., and Miki, T. (2011). Clinical course of patients with familial early-onset Alzheimer's disease potentially lacking senile plaques bearing the E693Δ mutation in amyloid precursor protein. Dement. Geriatr. Cogn. Disord. *32*, 45–54.

Takano, K., Kitao, Y., Tabata, Y., Miura, H., Sato, K., Takuma, K., Yamada, K., Hibino, S., Choshi, T., Iinuma, M., et al. (2007). A dibenzoylmethane derivative protects dopaminergic neurons against both oxidative stress and endoplasmic reticulum stress. Am. J. Physiol. Cell Physiol. *293*, C1884–C1894.

Tomiyama, T., Nagata, T., Shimada, H., Teraoka, R., Fukushima, A., Kanemitsu, H., Takuma, H., Kuwano, R., Imagawa, M., Ataka, S., et al. (2008). A new amyloid β variant favoring oligomerization in Alzheimer's-type dementia. Ann. Neurol. *63*, 377–387.

Tomiyama, T., Matsuyama, S., Iso, H., Umeda, T., Takuma, H., Ohnishi, K., Ishibashi, K., Teraoka, R., Sakama, N., Yamashita, T., et al. (2010). A mouse model of amyloid β oligomers: their contribution to synaptic alteration, abnormal tau phosphorylation, glial activation, and neuronal loss *in vivo*. J. Neurosci. *30*, 4845–4856.

Walsh, D.M., Klyubin, I., Fadeeva, J.V., Cullen, W.K., Anwyl, R., Wolfe, M.S., Rowan, M.J., and Selkoe, D.J. (2002). Naturally secreted oligomers of amyloid β protein potently inhibit hippocampal long-term potentiation *in vivo*. Nature *416*, 535–539.

Yagi, T., Ito, D., Okada, Y., Akamatsu, W., Nihei, Y., Yoshizaki, T., Yamanaka, S., Okano, H., and Suzuki, N. (2011). Modeling familial Alzheimer's disease with induced pluripotent stem cells. Hum. Mol. Genet. *20*, 4530–4539.

Journal of Human Genetics (2013) 58, 711–719

www.nature.com/jhg

ORIGINAL ARTICLE

YY1 binds to α-*synuclein* 3′-flanking region SNP and stimulates antisense noncoding RNA expression

Ikuko Mizuta[1,2], Kazuaki Takafuji[3], Yuko Ando[1], Wataru Satake[1], Motoi Kanagawa[1], Kazuhiro Kobayashi[1], Shushi Nagamori[3], Takayuki Shinohara[1], Chiyomi Ito[1], Mitsutoshi Yamamoto[4], Nobutaka Hattori[5], Miho Murata[6], Yoshikatsu Kanai[3], Shigeo Murayama[7], Masanori Nakagawa[8] and Tatsushi Toda[1]

α-*synuclein* (*SNCA*) is an established susceptibility gene for Parkinson's disease (PD), one of the most common human neurodegenerative disorders. Increased SNCA is considered to lead to PD and dementia with Lewy bodies. Four single-nucleotide polymorphisms (SNPs) in *SNCA* 3′ region were prominently associated with PD among different ethnic groups. To examine how these SNPs influence disease susceptibility, we analyzed their potential effects on *SNCA* gene expression. We found that rs356219 showed allele-specific features. Gel shift assay using nuclear extracts from SH-SY5Y cells showed binding of one or more proteins to the protective allele, rs356219-A. We purified the rs356219-A–protein complex with DNA affinity beads and identified a bound protein using mass spectrometry. This protein, YY1 (Yin Yang 1), is an ubiquitous transcription factor with multiple functions. We next investigated *SNCA* expression change in SH-SY5Y cells by YY1 transfection. We also analyzed the expression of antisense noncoding RNA (ncRNA) *RP11-115D19.1* in *SNCA* 3′-flanking region, because rs356219 is located in intron of *RP11-115D19.1*. Little change was observed in *SNCA* expression levels; however, *RP11-115D19.1* expression was prominently stimulated by YY1. In autopsied cortices, positive correlation was observed among *RP11-115D19.1*, *SNCA* and *YY1* expression levels, suggesting their functional interactions *in vivo*. Knockdown of *RP11-115D19.1* increased *SNCA* expression significantly in SH-SY5Y cells, suggesting its repressive effect on *SNCA* expression. Our findings of the protective allele-specific YY1 and antisense ncRNA raised a novel possible mechanism to regulate *SNCA* expression.
Journal of Human Genetics (2013) **58,** 711–719; doi:10.1038/jhg.2013.90; published online 12 September 2013

Keywords: α-*synuclein*; association; ncRNA; Parkinson's disease susceptibility; SNP; YY1

INTRODUCTION

Parkinson's disease (PD) (OMIM 168600) is one of the most common human neurodegenerative disorders, affecting 1–2% of people aged ⩾65 years.[1] Clinical features of PD (parkinsonism) include resting tremor, bradykinesia, rigidity and postural instability. PD is characterized pathologically by the loss of dopaminergic neurons in the substantia nigra of the midbrain and by the presence of intracellular inclusions known as Lewy bodies.[2]

Linkage studies for Mendelian-inherited PD have identified autosomal dominant genes, including α-*synuclein* (*SNCA*) and *LRRK2*, as well as the autosomal recessive genes *parkin*, *PINK1*, *DJ-1*, *ATP13A2*, *PLA2G6* and *FBXO7*.[3,4] However, Mendelian-inherited PD is rare compared with the far more common sporadic PD, a complex disorder caused by multiple genetic and environmental factors.[5]

SNCA was the first-identified causal gene for Mendelian-inherited PD.[6] The missense mutation A53T was identified in the original autosomal-dominant family, followed by confirmation of SNCA protein as a major component of Lewy bodies, the pathological hallmark of PD in both Mendelian-inherited and sporadic cases.[6,7] To date, three missense mutations and multiplication of *SNCA* have been identified in familial PD. Missense mutations are thought to increase the aggregation of SNCA protein. In patients with triplication of the *SNCA* locus, a doubling of wild-type *SNCA* gene dosage by triplication has been shown to result in the doubling of mRNA and protein expression in blood and in the brain.[8,9] Duplication of *SNCA* has also been implicated in familial PD. Patients with *SNCA* duplications show much milder clinical features than do those with *SNCA* triplications, more closely resembling sporadic cases.[10,11]

SNCA is also a causal gene for Mendelian-inherited dementia with Lewy bodies (DLB) (OMIM 127750). DLB, usually sporadic, is characterized clinically by dementia and parkinsonism and

[1]Division of Neurology/Molecular Brain Science, Kobe University Graduate School of Medicine, Kobe, Japan; [2]Department of Neurology, Graduate School of Medical Science, Kyoto Prefectural University of Medicine, Kyoto, Japan; [3]Division of Bio-system Pharmacology, Department of Pharmacology, Graduate School of Medicine, Osaka University, Suita, Japan; [4]Department of Neurology, Kagawa Prefectural Central Hospital, Takamatsu, Japan; [5]Department of Neurology, Juntendo University School of Medicine, Tokyo, Japan; [6]Department of Neurology, National Center Hospital, National Center of Neurology and Psychiatry, Kodaira, Japan; [7]Department of Neuropathology, Tokyo Metropolitan Institute of Gerontology, Tokyo, Japan and [8]North Medical Center, Kyoto Prefectural University of Medicine, Kyoto, Japan
Correspondence: Professor T Toda, Division of Neurology/Molecular Brain Science, Kobe University Graduate School of Medicine, 7-5-1 Kusunoki-chou, Chuo-ku, Kobe 650-0017, Japan.
E-mail: toda@med.kobe-u.ac.jp
Received 24 April 2013; revised 31 July 2013; accepted 2 August 2013; published online 12 September 2013

pathologically by widespread Lewy bodies. According to the overlapped features, PD and DLB are collectively called Lewy body diseases (LBD).

A popular hypothesis is that SNCA aggregation has a crucial role in neuronal loss and Lewy body formation and that increased SNCA leads to LBD. In this scenario, PD-associated *SNCA* polymorphisms might influence *SNCA* expression levels in sporadic PD. We and the others have previously reported that single-nucleotide polymorphisms (SNPs) in the *SNCA* 3′region were prominently associated with sporadic PD in both the Japanese and European populations.[12,13] Moreover, our recent genome-wide association study (GWAS) in the Japanese population,[14] as well as a GWAS analysis in individuals of European ancestry,[15] confirmed a strong association with the *SNCA* 3′region. In this report, we have examined how *SNCA* SNPs might influence LBD susceptibility.

MATERIALS AND METHODS

Genotyping

As described previously,[13] we recruited 882 unrelated sporadic PD patients (age: 64.9 ± 9.8 years; male/female ratio: 0.79) and 938 unrelated controls (age: 45.3 ± 16.3 years; male/female ratio: 1.10). The diagnosis of idiopathic PD was based on the presence of ⩾2 of the cardinal features of PD (tremor, rigidity, bradykinesia and postural instability), according to the criteria for sporadic PD.[16] Patients were evaluated by certified neurologists specializing in PD. The average age of onset was 57.4 ± 10.9 years. Forty-two patients showed early onset of PD (< 40 years of age), and 51 patients had a positive family history of PD. Patients who carried *parkin* mutations were excluded. All patients and controls were of Japanese ancestry. Informed consent was obtained from each individual, and approval for the study was obtained from the University Ethical Committees. Genomic DNA was extracted from the whole blood using FlexGene (Qiagen GmbH, Hilden, Germany). The rs356219, rs356220 and rs356203 SNPs were genotyped using TaqMan (Applied Biosystems, Lifetechnologies Corp., Carlsbad, CA, USA). SNPAlyze software (DYNACOM, Chiba, Japan) was used for pairwise linkage disequilibrium analysis (Lewontin's coefficient, D′, and standardized coefficient, *r*).

Luciferase assay

DNA fragments of ~250 bp corresponding to the regions containing four *SNCA* SNPs (rs356219, rs356220, rs356165 and rs356203) were amplified by PCR using heterozygous genomic DNA as template and then cloned into the SalI site of the pGL3-promoter vector (Promega Corporation, Madison, WI, USA). The orientation and allele identity of the insert were determined by DNA sequence analysis. Primer sequences used for PCR are listed in Supplementary Table 1. The human neuroblastoma cell line SH-SY5Y was grown in Dulbecco's Modified Eagle's medium supplemented with 10% fetal bovine serum and antibiotics. We transfected cells (3×10^5 cells per well on 24-well plates) with 360 ng of each construct and 40 ng of pRL-TK vector (Promega), as an internal control for transfection efficiency, using Effectene (Qiagen). After 48 h, cells were solubilized, and luciferase activity was measured using the dual luciferase assay system (Promega).

Preparation of nuclear extract

Nuclear extracts from SH-SY5Y cells were prepared as previously described, with minor modifications.[17] In brief, cells were washed and re-suspended in buffer A (10 mM 4-(2-hydroxyethyl)-1-piperazineethanesulfonic acid (HEPES)-KOH pH7.8, 10 mM KCl, 0.1 mM EDTA pH8.0, 0.1% NP-40, 1 mM dithiothreitol (DTT) and protease inhibitor cocktail (NACALAI TESQUE, Inc., Kyoto, Japan)). Nuclei were pelleted and re-suspended in buffer C (50 mM HEPES-KOH pH7.8, 420 mM KCl, 0.1 mM EDTA pH8.0, 5 mM $MgCl_2$, 2% glycerol, 1 mM DTT and protease inhibitor cocktail). After vortexing every 5 min for 30 min on ice, the samples were centrifuged, and the supernatants were used as nuclear extract.

Gel shift assay

Gel shift assays were performed as previously described.[18] SH-SY5Y nuclear extract (5–10 μg protein) was incubated with 0.031 pmol of 33-bp oligonucleotides (Supplementary Table 2) labeled with digoxigenin-11-ddUTP in 20 μl of binding buffer (20 mM HEPES pH7.6, 1 mM EDTA, 10 mM $(NH_4)_2SO_4$, 1 mM DTT, 0.2% Tween 20 and 30 mM KCl) containing 1 μg of poly(dI-dC) for 20 min, using the DIG gel shift kit (Roche Diagnostics, Mannheim, Germany). For competition studies, nuclear extract was pre-incubated with 3.85 pmol of unlabeled oligonucleotide before addition of the labeled probe. Supershift assays were performed by incubating the protein–DNA complexes with 0.8 μg of rabbit immunoglobulin G or rabbit polyclonal anti-YY1 (anti-Yin Yang 1; Active Motif, Carlsbad, CA, USA) for 5 min. The protein–DNA complexes were separated on DNA retardation polyacrylamide gels (Invitrogen, Lifetechnologies Corp., Carlsbad, CA, USA) and transferred to Hybond-N + Nylon membrane (GE Healthcare, Amersham Place, UK). All assays and gel electrophoresis procedures were performed at 4 °C. Signal detection was performed using the CSPD chemiluminescent detection system (Roche Diagnostics).

Ultraviolet (UV) cross-linking

The size of the rs356219-A binding protein was determined by UV cross-linking. We incubated 0.05 pmol of ^{32}P-labeled 33 bp rs356219-A oligonucleotide with SH-SY5Y nuclear extract and 6.16 pmol of unlabeled 33 bp competitor (rs356219-G or -A) for 15 min at 4 °C in the solution used for the gel shift assays. DNA–protein complexes were transferred to a flat-bottom 96-well plate, placed on a transilluminator and irradiated (312 nm, 15 min at 4 °C). Samples were run on 10% NuPAGE Novex Bis-Tris gels (Invitrogen), dried and autoradiographed.

Purification of the rs356219-A binding protein using affinity magnetic beads

Oligonucleotides containing rs356219-A with 5′-TCGA-3′ linkers were ligated in a head-to-tail manner and inserted into the SalI site of the pGL3-promoter vector (Promega). A fragment with 14 tandem repeats of rs356219-A was amplified from the plasmid by PCR using a biotin-labeled forward primer (5′-GGTAAAATCGATAAGGATCC-3′) and a non-labeled reverse primer (5′-TT GAAGGCTCTCAAGGGCAT-3′). The biotinylated PCR product (30 pmol) was bound to 1 mg of Dynabeads M-280 streptavidin (Dynal, Life Technologies, Carlsbad, CA, USA). Fifty microliters of SH-SY5Y nuclear extract, prepared with Buffer C containing 200 mM KCl, was precleared in 1 ml of binding buffer in the presence of 1 mg of unbound beads and 144 pmol of 33 bp non-labeled competitor rs356219-A or -G. Following magnetic separation, the supernatant was incubated with 1 mg of probe-bound Dynabeads for 30 min at 4°C. The beads were washed five times and then eluted sequentially, twice with 40 μl elution buffer (20 mM HEPES-KOH pH7.6, 1 mM EDTA, 10 mM $(NH_4)_2SO_4$, 1 mM DTT, 0.2% Tween 20, protease inhibitor cocktail and 10% glycerol) containing 200 mM KCl and twice with 40 μl elution buffer containing 300 mM KCl. Proteins in each elute were analyzed by electrophoresis on 10% NuPAGE Novex Bis-Tris gel (Invitrogen). Binding activity of each elute was evaluated by gel shift assay.

In-gel digestion

Protein bands were excised from a silver-stained gel. Proteins were digested with sequencing grade-modified trypsin (Roche Diagnostics) as described elsewhere.[19] Tryptic peptides were extracted from gel pieces in 50% acetonitrile with 5% formic acid and dried using a vacuum centrifuge. Dried peptides were resuspended in 5% acetonitrile containing 0.1% trifluoroacetic acid and desalted using StageTips with a C18 Empore disk membrane (3M, Minneapolis, MN, USA) according to the published procedure.[20]

Liquid chromatography-tandem mass spectrometry (LC-MS/MS) and data analysis

LC-MS/MS analysis was performed using a Paradigm MS4 nanoHPLC system (Michrom BioResources, Inc., Auburn, CA, USA) coupled to a LTQ linear ion trap mass spectrometer (Thermo Electron Corp., Waltham, MA, USA) with a

nanoelectrospray ionization source (AMR Inc., Tokyo, Japan). Tryptic peptides were injected by a HTC-PAL autosampler (CTC Analytics, Zwingen, Switzerland) and enriched on a C18 trap column (300 μm I.D. × 5 mm length, CERI, Tokyo, Japan) at a flow rate of 6 μl min^{-1}. The samples were subsequently separated by a C18 reverse phase column (100 μm I.D. × 150 mm length, Nikkyo Technos, Tokyo, Japan) at a flow rate of 1 μl min^{-1}, with a linear gradient from 2% to 65% mobile phase B, that is; from 98% to 35% of mobile phase A. The mobile phase B consisted of 95% acetonitrile with 0.1% formic acid, whereas the mobile phase A consisted of 2% acetonitrile with 0.1% formic acid. LC-MS/MS analysis was carried out using a data-dependent triple-play mode. Automated gain control values were set at 1.5×10^4, 1.5×10^3 and 5.0×10^3 for Full-MS, Zoom-MS and MS/MS, respectively. A spray voltage of 2.4 kV was applied. The MS scan range was *m/z* 300–2000. Peptides and proteins were identified by Mascot software ver. 2.2 (Matrix Science, London, UK), screened against the most recent version of the human IPI database from EMBL-EBI (http://www.ebi.ac.uk/IPI/IPIhuman.html). Maximum tolerance was set to 1.2 Da for MS data, 0.5 Da for MS/MS data and strict trypsin specificity allowing for up to one missed cleavage. Carbamidomethylation of cysteine and oxidation of methionine were allowed as variable modifications.

Transfection of YY1

SH-SY5Y cells were transfected with pCMV6-XL5 expressing human YY1 (OriGene, Rockville, MD, USA) or blank vector by using an electroporator CUY21 *Pro-Vitro* (NEPA GENE, Chiba, Japan). Twenty-four hours after transfection, the cells were harvested. For western blotting, whole-cell lysates were separated by electrophoresis on 10% NuPAGE Novex Bis-Tris gel and blotted onto PVDF membrane (Immobilon-P, Merck Millipore, Darmstadt, Germany). The membranes were incubated with anti-YY1 (sc-1703, Santa Cruz Biotechnology, Santa Cruz, CA, USA) or anti-Actin (sc-10731, Santa Cruz Biotechnology), followed by reaction with horseradish peroxidase-conjugated secondary antibodies. Signal detection was performed using the ECL detection system (Thermo Fisher Scientific, Rockford, IL, USA).

Overexpression/knockdown of *RP11-115D19.1*

For overexpression experiment, *RP11-115D19.1-003* cDNA (469 bp) was amplified from SH-SY5Y cDNA and *RP11-115D19.1-005* cDNA (567 bp) was synthesized (Genscript, Piscataway, NJ, USA). Each fragment was cloned into pCMV6-XL5 and transfected to SH-SY5Y cells as described above. For repression experiment, siRNA targeting to *RP11-115D19.1* (5′-CATGCTTC-CAGAGAATGCATATTCT-3′) was designed from the common region between *RP11-115D19.1-003* and *-005*. The siRNA and negative control (Lo GC duplex) were purchased (Stealth RNAi, Invitrogen) and transfected as described above. Twenty-four hours after transfection, the cells were harvested.

Real-time reverse transcription-PCR (RT-PCR)

As described previously, autopsied frontal cortices were obtained from the Brain Bank for Aging Research (Tokyo Metropolitan Geriatric Hospital/Tokyo Metropolitan Institute of Gerontology) and Department of Neurology, Juntendo University School of Medicine, Tokyo, Japan. The samples contained 21 cases (age, 82.6 ± 7.1 (s.d.) years; 11 males and 10 females) with Lewy body pathology defined by the third Consensus Guideline for Dementia with Lewy Bodies, comprising PD with and without dementia and DLB and 18 control subjects (age, 81.2 ± 5.2 years; 12 males and 6 females) without parkinsonism or dementia and without neurodegenerative pathological changes. Total RNA was extracted from SH-SY5Y cells or tissue using RNeasy (Qiagen), and cDNA was prepared using High Capacity RNA-to-cDNA kit (Applied Biosystems). Real-time RT-PCR was carried out on StepOnePlus real-time PCR system (Applied Biosystems) using Fast SYBR Green Master Mix (Applied Biosystems). First-strand cDNA was amplified using primers specific for *SNCA* (forward; 5′-CAGAAGCAGCAGGAAAGACA-3′, reverse; 5′-CCACTGCTCCT CCAACATTT-3′, product size; 132 bp), *RP11-115D19.1-003* (forward; 5′-TAA AACCTGCAAATTCACATCTTC-3′, reverse; 5′-AAGTAGGTAAGTAGGGCAG TGCAT-3′ product size; 133 bp), *RP11-115D19.1-005* (forward; 5′-CCATGCTT CCAGAGAATGCA-3′, reverse; 5′-GTGCTTCCCTTTCACTGAAG-3′, product size; 144 bp), *GAPDH* (forward; 5′-CATCTTCCAGGAGCGAGATC-3′, reverse; 5′-TGCAAATGAGCCCCAGCCTT-3′, product size; 114 bp), *NF* (*neurofilament L*, forward; 5′-AAGAACACCGACGCCGTGCG-3′, reverse; 5′-TGCCATTTCACTCTTTGTGG-3′, product size; 222 bp), and *YY1* (forward; 5′-TGGCAAAGCTTTTGTTGAGA-3′, reverse; 5′-ATGTGTGCGCAAATTGA AGT-3′, product size; 130 bp). For quantification, we used a relative standard curve method and amplified cDNA corresponding to 100 ng (*RP11-115D19.1*) or 1.7 ng (*SNCA*, *GAPDH*, and *NF*) RNA per well. Standard curves were generated from amplification of diluted series of cDNA from cortices (*SNCA*, *GAPDH*, and *NF*), YY1-transfected SH-SY5Y cells (*RP11-115D19.1*) or plasmids (pCMV-YY1, pCMV-RP11-115D19.1-003, pCMV-RP11-115D19.1-005). *SNCA*, *RP11-115D19.1* and *YY1* expression levels were normalized to those of *GAPDH* (SH-SY5Y cells) or *NF* (cortices). The values were determined in triplicate or duplicate. Genotyping of rs356219 of SH-SY5Y and cortices was performed using restriction fragment length polymorphism and sequencing.

RESULTS

Identification of four *SNCA* SNPs associated with PD in both the Japanese and European populations

We previously identified six SNPs (rs3857053, rs356165, rs7684318, rs3775424, rs3796661 and rs2737029), located in the 3′-flanking, 3′-UTR and intron 4 of *SNCA*, that were prominently associated with PD.[13] Independently, analysis of a European population also reported

Table 1 PD-associated *SNCA* SNPs reported in the Japanese and German studies

	Position	*Region*	*Japanese study*[a]		*German study*[b]		*MAF of Europeans in the dbSNP database*		
SNP ID	*(NCBI build 36)*		*P-value*	*MAF (Case/control)*	*P-value*	*MAF (Case/control)*	*HapMap-CEU*	*EGP_CEPH_PANEL*	*AFD_EUR_PANEL*
rs356219	90637601	3′-Flanking	7.3×10^{-9}	0.34/0.43	0.00467	0.46/0.38	0.425		0.354
rs356220	90641340	3′-Flanking	8.7×10^{-10}	0.33/0.43	0.00485	0.46/0.38	0.427		
rs3857053	90645674	3′-Flanking	1.1×10^{-9}	0.33/0.43				0.071	
rs356165	90646886	3′-UTR	2.0×10^{-9}	0.33/0.43	0.00555	0.46/0.38	0.433	0.412	
rs7684318	90655003	Intron 4	5.0×10^{-10}	0.33/0.43					0.024
rs3775424	90665256	Intron 4	5.4×10^{-10}	0.33/0.43			0.033		
rs356203	90666041	Intron 4	1.4×10^{-7}	0.34/0.43	0.00548	0.46/0.38		0.45	
rs3796661	90687507	Intron 4	2.7×10^{-9}	0.33/0.42			0.033		0.021
rs2737029	90711770	Intron 4	1.7×10^{-11}	0.32/0.42	0.09994	0.46/0.42	0.45		0.396

Abbreviations: MAF, minor allele frequency; NCBI, National Center for Biotechnology Information; PD, Parkinson's disease; *SNCA*, α-*synuclein*; SNP, single-nucleotide polymorphism; UTR, untranslated region.
[a]From our previous study[13] and present study (rs356219, rs356220 and rs356203).
[b]From the previous German study[12] (replication sample set II).

strong association for four SNPs (rs356219, rs356220 rs356165, rs356203) in the 3′-flanking region of *SNCA*.[12] Of these SNPs, only rs356165 was common to the two studies. We genotyped the remaining SNPs of the European population (rs356219, rs356220 and rs356203) and confirmed their prominent association with the Japanese population (Table 1, Figure 1a). The remaining SNPs reported in the Japanese population study were rare in the European population (Table 1, Figure 1a). From these findings, we concluded that rs356219, rs356220, rs356165 and rs356203 were associated prominently with PD in both the populations. Our functional analysis focused on these four SNPs.

Allele-specific effect of rs356219 in luciferase and gel shift assays

To determine whether the four SNPs could affect *SNCA* expression levels, we constructed plasmids containing genomic fragments with each SNP, placed downstream from a luciferase transcriptional unit (Figure 1b). For rs356219, the clone containing the protective A allele showed 1.6-fold greater luciferase activity than did the disease-associated G allele. We observed no allele-specific differences for the remaining three SNPs, however. Next, we used gel shift assays to examine the possibility that proteins might bind to the SNPs in an allele-specific manner (Figure 1c). The protective rs356219-A allele showed an intense shift band relative to the disease allele rs356219-G. Alleles of rs356220 and rs356165 showed similar shift band intensities. For rs356203, the intensity of the C disease allele was stronger than that of the protective T allele. We focused our subsequent analyses on rs356219, which was the only SNP that showed allele-specific features in both the assays.

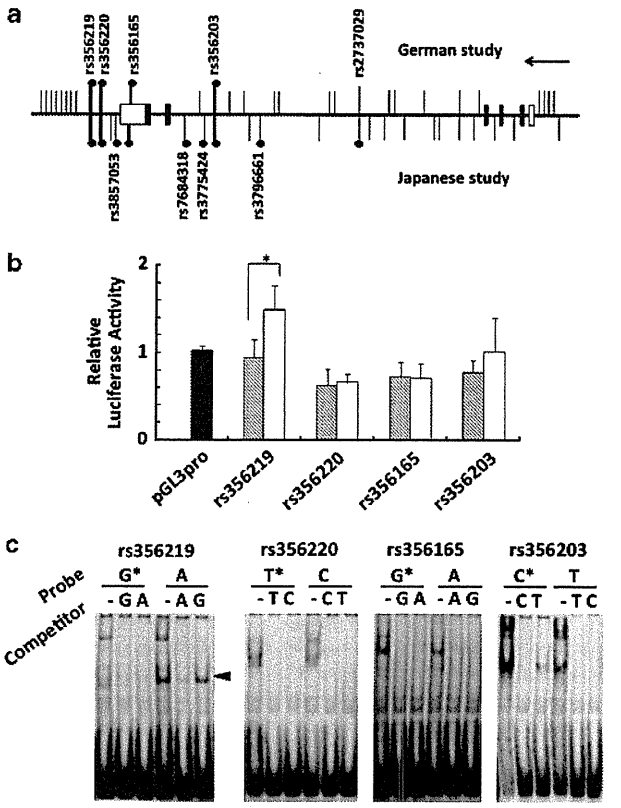

Figure 1 Transcriptional regulatory activity affected by *SNCA* SNPs. (**a**) Schematic representation of the *SNCA* gene with relative positions of SNPs genotyped in the Japanese and European population studies. The *SNCA* locus (horizontal line), coding regions (black boxes), 5′- and 3′-UTR (white boxes) and transcription orientation (arrow) are shown. The relative positions of SNPs (vertical lines) genotyped in the Japanese study (lower) and the German study (upper) are represented. Of the SNPs strongly associated with each study (solid circle), four SNPs are commonly associated with PD in both the studies (thick vertical lines). (**b**) Luciferase assay. Luciferase activities relative to the control pGL3-promoter construct (black bar) were compared between disease allele (shaded) and protective allele (white) at each of the four SNPs ($n=7$). Luciferase activity of the protective rs356219-A allele was significantly increased relative to that of the G disease allele (*$P=0.001$ by Student's t-test). (**c**) Gel shift assay. Binding of SH-SY5Y nuclear protein to alleles at the four SNPs are presented. Shift bands were compared between the disease allele (*) and the protective allele at each SNP. The intense shift band observed for the protective allele rs356219-A was competed by non-labeled competitor allele A but not by the disease allele G (arrowhead).

Identification of the rs356219-A binding protein

We performed UV-crosslinking and estimated the size of the protein bound to the rs356219-A allele at ~55 kDa (Figure 2a). Next, we purified the protein by binding to rs356219-A affinity beads in the presence of non-biotinylated rs356219-G fragments as a competitor. Control experiments used non-biotinylated rs356219-A fragments as competitor. After washing, the binding protein was eluted sequentially, twice with elution buffer containing 200 mM KCl and twice with buffer containing 300 mM KCl. Electrophoresis and gel shift assay located the ~55 kDa band and binding activity within the second (200 mM KCl) and third (300 mM KCl) elutes. Both were absorbed by the rs356219-A competitor in the control experiments (Figure 2b). Subsequent LC-MS/MS analysis showed that peptides derived from a transcription factor YY1 were identified from the ~55 kDa bands (Figure 2c). We concluded that the rs356219-A binding protein was YY1. This observation was confirmed by super-shift assays using anti-YY1 antibody (Figure 2d, Supplementary Figure 1).

Effects of YY1 transfection on *SNCA* and noncoding RNA (ncRNA) *RP11-115D19.1* expression in SH-SY5Y cells

Luciferase assay and gel shift assay suggested that YY1 bound to rs356219 protective allele and stimulated transcription (Figures 1b and c and 2). Recent Ensemble Genome Browser showed antisense ncRNA named *RP11-115D19.1* in *SNCA* 3′-flanking region. The SNP rs356219 locates intron of its two spliced isoforms (*RP11-115D19.1-003* and *-005*; Figure 3a), suggesting that rs356219 might influence transcription of *SNCA* and/or *RP11-115D19.1*. If rs356219 influences *SNCA* promoter, increased luciferase activity in the protective allele (Figure 1b) appears incompatible with the hypothesis that increased SNCA leads to PD. To address this issue, we investigated YY1-induced expression of *SNCA* and *RP11-115D19.1* in SH-SY5Y neuroblastoma cells, whose genotype of rs356219 was heterozygous. YY1 transfection showed 23-fold increase in *RP11-115D19.1-003*, 24-fold increase in *RP11-115D19.1-005* and twofold increase in *SNCA* expression levels (Figure 3b). Other two independent transfection experiments replicated the prominent stimulation of *RP11-115D19.1* by YY1; however, they showed little changes of *SNCA* expression (data not shown). We analyzed allele-specific expression level of *SNCA* by using 3′-UTR SNP rs356165 as a marker and found little difference between the alleles, both in YY1 and blank transfection (Figure 3c). We could not analyze allele-specific expression of *RP11-115D19.1*, because no SNP was found in *RP11-115D19.1* exons in SH-SY5Y. Although the role of *RP11-115D19.1* on *SNCA* expression remains uncovered, increased luciferase activity in the

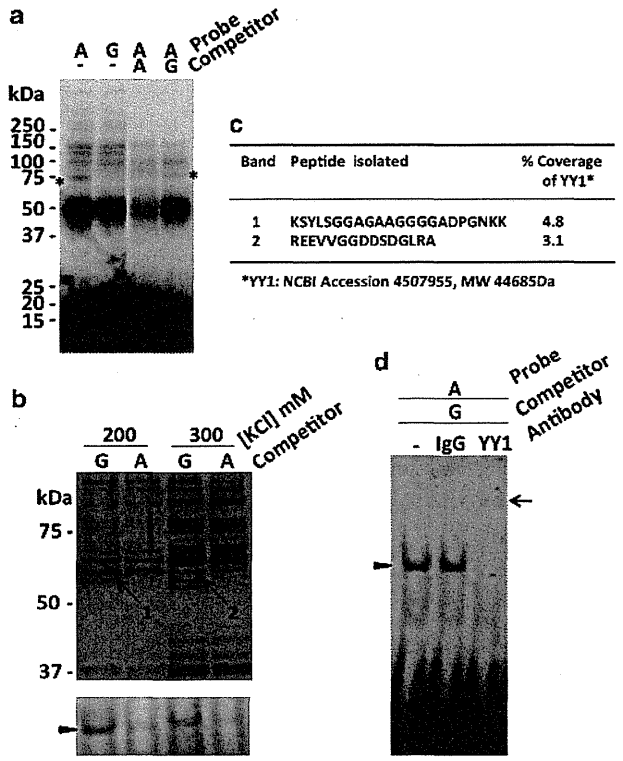

Figure 2 Purification and identification of the rs356219-A binding protein. (a) Estimation of the molecular size of the rs356219-A binding protein by UV cross-linking analysis. SH-SY5Y nuclear extract was incubated with the probe, rs356219-A (protective allele) or rs356219-G (disease allele) in the presence or absence of non-labeled competitor. Following UV irradiation, the cross-linked protein–probe complexes were analyzed by SDS-PAGE. The size of allele A and protein complex was estimated as ~70 kDa (*). As the mean size of the free probe was estimated as ~15 kDa, the protein of interest was estimated as ~55 kDa. (b) Purification of the rs356219-A binding protein using DNA affinity beads. Nuclear extract from SH-SY5Y cells was incubated with affinity beads bound to tandem repeats of 33 bp region containing the A allele, in the presence of free competitor G allele (for purification) or control allele A. After the binding reaction, beads were washed and eluted twice with buffer containing 200 mM KCl and then twice with buffer containing 300 mM KCl. Aliquots of each elution were analyzed by SDS-PAGE (upper panel) and gel shift assays using rs356219-A as a probe (lower panel). The second and third elutions are shown. The rs356219-A binding band of ~55 kDa was observed (bands 1 and 2, arrows) and correlated with the intensity of the gel shift band (arrowhead). (c) Summary of mass spectrometry analysis of the two ~55 kDa bands. Peptides derived from YY1 were identified from both bands. (d) Supershift assay using anti-YY1 antibody. After binding of the rs356219-A probe and SH-SY5Y nuclear extract in the gel shift assay, anti-YY1 antibody was added and analyzed by electrophoresis. The shift band (arrowhead) was supershifted by anti-YY1 antibody (arrow), confirming that the shift band contains YY1.

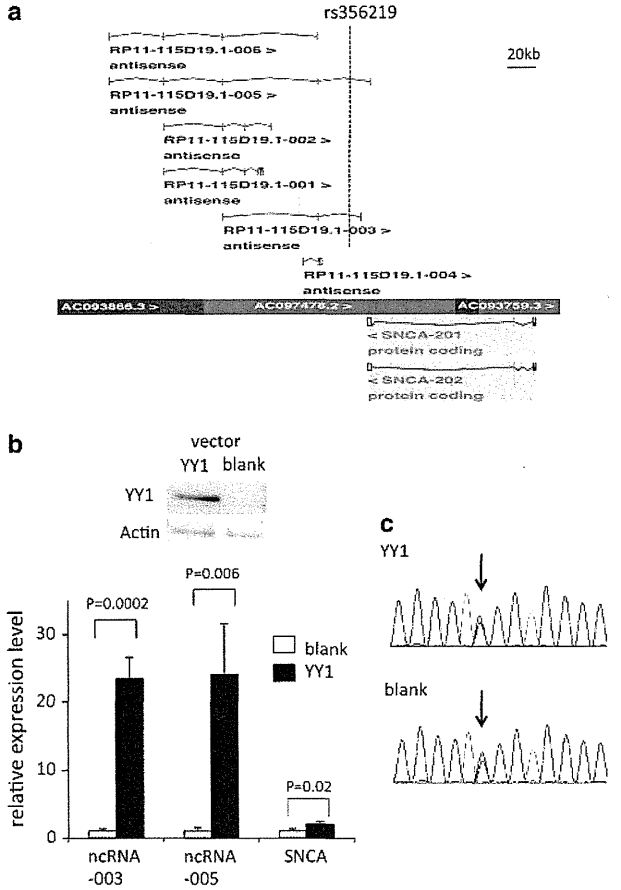

Figure 3 *SNCA* and its 3′-flanking ncRNA expression in YY1-transfected SH-SY5Y cells. (a) Genomic structure of *SNCA* and its 3′-flanking region (Ensemble Genome Browser). SNP rs356219 locates in intron of *RP11-115D19.1-003* and *-005* (dotted line). (b) Quantification of *SNCA* mRNA and two spliced isoforms of *RP11-115D19.1* ncRNA (*-003* and *-005*) in SH-SY5Y cells transfected by YY1 expression vector or blank vector. Overexpression of YY1 was confirmed by western blot analysis (upper). Three YY1 plates and three blank plates were quantified. Mean values of three YY1 plates (black bar) relative to the mean of three blank plates (white bar) are shown with s.d. (lower). YY1 transfection showed 23-fold increase in *RP11-115D19.1-003*, 24-fold increase in *RP11-115D19.1-005* and twofold increase in *SNCA* expression levels. (c) Semiquantitative analysis of allele-specific expression of *SNCA* 3′-UTR. Sequencing chromatograms of SH-SY5Y RT-PCR products of *SNCA* 3′-UTR containing rs356165 (arrow) are shown. Little difference between the heights of allele-C and allele-T was observed, both in the YY1 and blank transfection.

protective allele is not contradictory to YY1-stimulated expression of *RP11-115D19.1*.

SNCA, ncRNA *RP11-115D19.1* and *YY1* expression in relation to rs356219

We found the possibility that rs356219 may influence expression of *RP11-115D19.1* from *in vitro* and cellular experiments (Figures 1–3). To extend the findings, we investigated *SNCA* and *RP11-115D19.1* expression in relation to rs356219 genotypes in autopsied brain tissues. We previously reported that *SNCA* expression levels tended to be positively correlated with the number of the disease allele of rs7684318 in autopsied cortices.[13] Because rs356219 and rs7684318 are in a tight linkage disequilibrium group (Supplementary Table 3), our previous finding is to be replicated in relation to rs356219. Actually, rs356219 genotypes were completely correlated with those of rs7684318 in our autopsied samples. Moreover, we synthesized new cDNAs and quantified *SNCA* expression levels by real-time RT-PCR to compare among rs356219 genotypes. Although the difference among genotypes did not reach significance, we confirmed similar tendency with our previous report; mean of *SNCA* mRNA was lowest in AA (homozygote of protective alleles) either in cases, controls and combined (Supplementary Figure 2a). We also analyzed *RP11-*

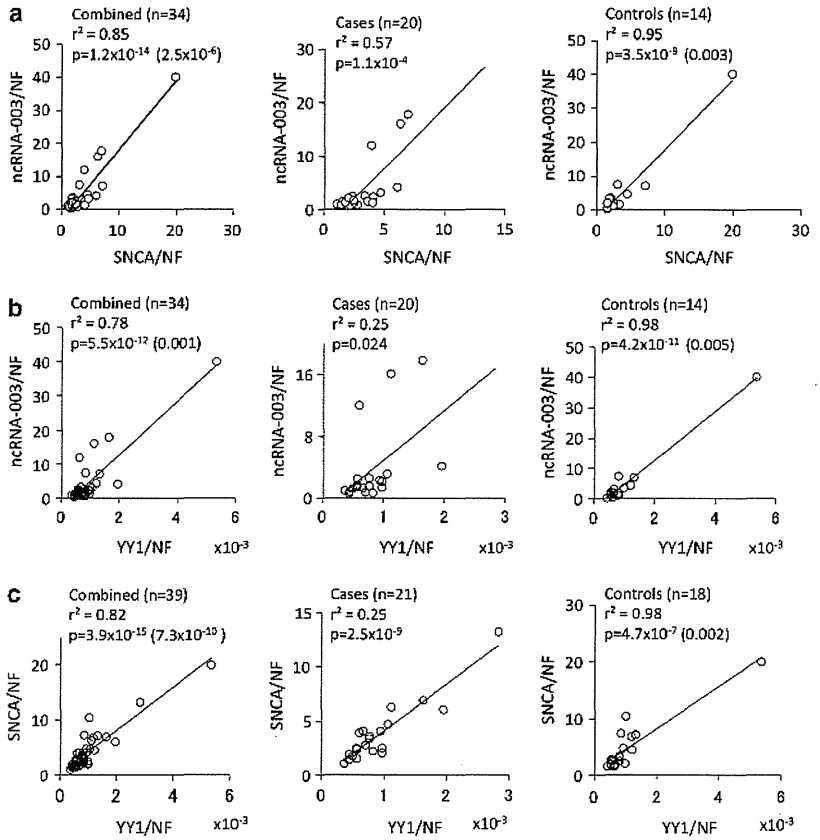

Figure 4 Correlation of SNCA, its 3′-flanking ncRNA and YY1 expression levels in autopsied frontal cortices. Scatterplots of *SNCA* versus *RP11-115D19.1-003* (**a**), *YY1* versus *RP11-115D19.1-003* (**b**) and *YY1* versus *SNCA* (**c**) expression levels (standardized by NF in arbitrary units). Plots are shown in all the samples (combined), cases and controls separately. Linear regression lines are indicated with r^2 and *P* values (Pearson's correlation analysis). Even after excluding the outliner in the controls, the strong correlations remain (*P*-values are in parenthesis).

115D19.1 expression in relation to rs356219. *RP11-115D19.1-005* expression levels in 38 out of the 39 cortices were too low to be quantified (data not shown); however, those of *RP11-115D19.1-003* could be quantified in 34 cortices. Compared with *SNCA*, mean values of *RP11-115D19.1-003* expression levels showed little difference among rs356219 genotypes (Supplementary Figure 2b). However, it was notable that *RP11-115D19.1-003* expression levels were strongly and positively correlated with those of *SNCA* (Figure 4a). Even after excluding the outliner in the controls, the strong correlation remained ($P = 2.5 \times 10^{-6}$ in combined and $P = 0.003$ in controls). We also examined *YY1* mRNA expression levels in cortical tissues. *YY1* expression levels were normalized by those of *NF*, because previous immunohistochemical study in an adult rodent brain reported that YY1 were strongly expressed in neurons and not detected in astrocytes.[21] *YY1* expression levels showed no significant difference among rs356219 genotype (Supplementary Figure 2c); however, positive correlation between *YY1* and *RP11-115D19.1-003* (Figure 4b) was compatible to the YY1-induced ncRNA expression shown in cellular YY1-overexpression experiment (Figure 3).

Effects of overexpression/knockdown of ncRNA *RP11-115D19.1* on *SNCA* expression in SH-SY5Y cells

Positive correlation between *SNCA* and *RP11-115D19.1* in the brain suggests regulatory roles of *RP11-115D19.1* on the *SNCA* expression. To address this issue, we investigated *SNCA* expression levels in SH-SY5Y cells transfected by *RP11-115D19.1* expressing vectors or siRNA designed from a common region of *RP11-115D19.1-003* and *-005*. Overexpression of *RP11-115D19.1* did not affect *SNCA* expression levels significantly (Figure 5a). On the contrary, siRNA-mediated knockdown (~90%) of *RP11-115D19.1* increased *SNCA* expression levels significantly (1.2-fold, $P = 0.0014$) (Figure 5b), which was replicated in three independent knockdown experiments (data not shown). These findings suggest that *RP11-115D19.1* may have repressive effect on the *SNCA* expression.

DISCUSSION

Recent GWAS have provided new information regarding PD susceptibility genes.[14,15] Our GWAS analysis in the Japanese population confirmed strong associations at *SNCA* and *LRRK2* and identified novel susceptibility loci, including *PARK16* (1q32) and *BST1* (4p15).[14] GWAS in individuals of European ancestry confirmed strong associations at *SNCA*, *MAPT* and *LRRK2*, and also confirmed *PARK16* as a novel locus.[15] Following meta-analysis of GWAS in the European ancestry populations confirmed *BST1* susceptibility.[22] Susceptibility associated with *MAPT* was not consistent between the populations, in part because of ethnic differences in allele frequencies. For example, a strong association for the H1/H2 haplotype of *MAPT* (OMIM 157140) has been reported in Caucasians,[23] but this observation has not been replicated in Asians. The frequency of the H2 haplotype is

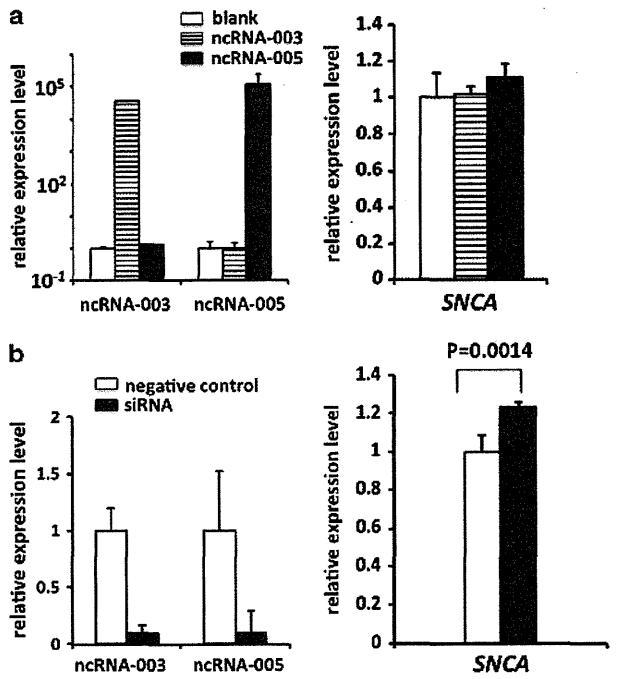

Figure 5 *SNCA* expression in SH-SY5Y cells after overexpression/knockdown of the ncRNA. (**a**) Quantification of *SNCA* mRNA in SH-SY5Y cells transfected by *RP11-115D19.1 ncRNA-003* and *-005* expression vectors or blank vector. Mean values of three *ncRNA-003* plates (striped bar) or three *ncRNA-005* (black bar) plates relative to the mean of three blank plates (white bar) are shown with s.d. Overexpression (over 10000-fold) of *ncRNA-003/-005* was confirmed (left). *SNCA* expression did not change significantly by transfection of *ncRNA-003* ($P=0.83$, versus blank, *t*-test) or *ncRNA-005* ($P=0.28$, versus blank, *t*-test) (right). (**b**) Quantification of *SNCA* mRNA in SH-SY5Y cells transfected by siRNA targeted to *RP11-115D19.1* or negative control RNA. Mean value of four siRNA plates (black bar) relative to the mean of four control plates (white bar) are shown with s.d. Repression of the *ncRNA-003/005* (~0.1-fold) was confirmed (left). *SNCA* expression increased significantly (~1.2-fold, $P=0.0014$, *t*-test) by transfection of siRNA (right).

approximately 20% in Caucasians but almost absent in Asians.[24] On the contrary, *SNCA*, *LRRK2*, *BST1* and *PARK16* susceptibilities are consistent in both the populations. To examine how SNPs might affect disease susceptibility, we focused on the *SNCA* SNPs that associate with PD across different ethnicities.

Of the four SNPs analyzed, only rs356219 showed distinct allele-specific features. The protective A allele showed greater activity in lucifersae assays than did the disease allele G. Moreover, specific binding of a nuclear protein to the protective A allele was observed using gel shift assays. When purified, this protein was identified as the transcription factor YY1, a ubiquitous zinc-finger transcription factor belonging to the Drosophila-Polycomb group protein family. The name Yin Yang 1 reflects its dual effects on transcriptional regulation, as YY1 can stimulate or repress gene expression depending on the cellular context. YY1 is associated with multiple biological functions such as proliferation, differentiation, apoptosis and tumorigenesis.[25,26] Comparison with known YY1 consensus binding motifs[27] supports the idea that the sequence of rs356219 would alter YY1 affinity in an allele-specific manner (Supplementary Figure 1). Based on the hypothesis that increased SNCA leads to LBD, it is reasonable to presume that YY1 could diminish *SNCA* gene expression levels by binding to the protective allele. However, elevated luciferase activity of the construct containing the rs356219-A protective allele seems contradictory. To address this issue, we transfected YY1 expression vector to human neuroblastoma cell line SH-SY5Y of which rs356219 genotype is GA and compared allele-specific expression level using 3′-UTR SNP rs356165 as a marker. YY1 was successfully overexpressed in SH-SY5Y and little difference of *SNCA* expression levels between the alleles was observed (Figure 3c), suggesting little possibility of allele-specific transcription regulation by YY1–rs356219 interaction, at least in SH-SY5Y cells. We raised another possibility that rs356219 might influence transcription of a certain gene regulating *SNCA* expression. Recent Ensemble Genome Browser (http://www.ensembl.org/) showed novel antisense ncRNA *RP11-115D19.1* in *SNCA* 3′-flanking region. We also investigated the expression of *RP11-115D19.1*, because rs356219 is located in introns of the two spliced isoforms, *RP11-115D19.1-003* and *-005* (Figure 3a). Surprisingly, *RP11-115D19.1* expression was prominently stimulated by YY1 overexpression, in contrast to the little change in *SNCA* expression (Figure 3b). From these findings, it would be informative to analyze *RP11-115D19.1* expression levels stimulated by YY1 in relation to rs356219 genotypes. Because no SNP was found in SH-SY5Y *RP11-115D19.1* exons, we designed an experiment to transfect YY1 expression vector to human lymphoblasts G or A in rs356219 and compare *SNCA* mRNA expression levels between G and A. However, because of low transfection efficiency (~10% by electroporation), we could not induce YY1 in lymphoblasts (data not shown).

Our *in vitro* and cellular experiments showed the possibility that rs356219 might influence YY1-stimulated transcription of *RP11-115D19.1*. To extend this, we investigated steady state *SNCA* and *RP11-115D19.1* expression levels in autopsied frontal cortices in relation to rs356219 genotypes. *SNCA* expression levels in cortices tended to be positively correlated with the number of the disease allele of rs356219 (Supplementary Figure 2a), replicating our previous result.[13] Our result was not consistent with other groups' previous reports. Fuchs *et al.*[28] reported that higher *SNCA* mRNA correlated with rs356219 disease allele in the substantia nigra of the midbrain, however, with the protective allele in the cerebellum. On the other hand, Linnertz *et al.*[29] reported that higher *SNCA* mRNA correlated with rs356219 protective allele in the temporal cortices and midbrain and unchanged among the genotypes in the frontal cortices. The discrepancies among these studies might be from the number and variation of samples.

We also analyzed steady state *in vivo* *RP11-115D19.1* expression levels and found little difference among genotypes (Supplementary Figure 2b). However, it was of note that *RP11-115D19.1* expression levels were strongly and positively correlated with those of *SNCA* (Figure 4a). Recent reports focused on SNP-coexpression associations.[30,31] We found a positive correlation between *SNCA* and *RP11-115D19.1* in either of the rs356219 genotype. The significance of correlation tended to increase according to the number of the disease allele G (Supplementary Figure 3). To confirm this tendency, large number of samples must be analyzed.

We also quantified *RP11-115D19-003* and *SNCA* mRNA levels in lymphoblasts originated from PD patients harboring GG and AA (Supplementary Figure 4). Similarly to the brain, there were no significant differences in *RP11-115D19-003* and *SNCA* expression levels between GG and AA lymphoblasts. In contrast to the brain, however, there was no significant correlation between *RP11-115D19-003* and *SNCA* levels in lymphoblasts. Although the numbers examined were limited, these results suggest interaction between *RP11-115D19* and *SNCA* expressions may be brain-specific.

The coexpression suggests functional interaction between the two genes. *RP11-115D19.1* transcripts span 0.4–1.8 kb, classified by size to long noncoding RNAs (lncRNAs).[32] Although the function of majority of lncRNAs remains uncovered, some are supposed to participate in regulating transcription of coding genes. For example, it was reported that mRNA of *BACE1*, *β-site APP (amyloid precursor protein) cleaving enzyme 1*, was stabilized by *BACE1* antisense transcript, a lncRNA including an exon complementary to a *BACE-1* exon.[33] On the contrary, recent work reported that *brain-derived neurotrophic factor* (*BDNF*) was repressed by its antisense RNA transcript.[34] These reports showed that some antisense ncRNAs downregulated and others upregulated transcription of the sense genes. *RP11-115D19.1-005* transcript overlaps *SNCA* 3′-UTR partly in tail-to-tail manner (Figure 3a), suggesting putative regulatory activity on *SNCA* expression. *RP11-115D19.1-005* transcript was hardly detected in steady state brain mRNA; however, it was prominently stimulated by YY1 in SH-SY5Y cells, as well as in *-003* transcript.

To investigate how *RP11-115D19.1* may influence *SNCA* expression, we performed cellular overexpression and knockdown experiments. We found that siRNA-mediated knockdown of the ncRNA increased *SNCA* expression (~ 1.2-fold) in SH-SY5Y cells (Figure 5b). The effect seems small; however, it could be sufficient to influence susceptibility to late-onset sporadic PD and DLB, caused by multiple genetic and environmental factors. The reason why overexpression of the ncRNA did not suppress *SNCA* expression remains unknown. We hypothesize that ncRNA may influence *SNCA* expression in a locus-dependent manner and that repressive effect may be saturated at endogeneous (low) expression level of ncRNA.

We performed similar analysis using human embryonic kidney-derived HEK293 cells. YY1-induced expression of ncRNA was replicated in HEK293 cells (Supplementary Figure 5). The degree of ncRNA stimulation in HEK293 cells, however, was smaller than those in SH-SY5Y cells. *SNCA* expression levels in HEK293 cells did not change significantly after YY1 overexpression, ncRNA overexpression or ncRNA knockdown. These suggest that ncRNA's repressive effect on *SNCA* expression may be specific to neuroblastoma cells.

Based on our demonstration that ncRNA has directly repressive effect on *SNCA* expression *in vitro*, positive correlation between *SNCA* and its antisense ncRNA *in vivo* may be explained as follows: One possibility is that expression of antisense ncRNA may coordinate with that of sense gene *SNCA* under locus-specific transcriptional regulation. Another possibility is that certain neurotoxic factors, including oxidative stress, may cause stimulation of *SNCA* and ncRNA expression levels simultaneously. Simultaneous stimulation of *SNCA* and *YY1* may be also possible, because of correlation of *SNCA* and *YY1* expression levels in the brain (Figure 4c) and YY1-induced expression of ncRNA in cells (Figure 3). In both the hypotheses (Supplementary Figure 6), ncRNA may be beneficial to maintain *SNCA* expression levels within normal range.

Accumulation of SNCA is thought to be neurotoxic. On the other hand, the protective effects of SNCA are also reported. Chandra *et al.*[35] reported that transgenic expression of *SNCA* rescued neurodegeneration in *CSPα* knockout mice. Musgrove *et al.*[36] reported that endogeneous SNCA upregulation in response to weak oxidative stress was neuroprotective against additional acute oxidative stress in primary cultured neurons. These suggest that SNCA exerts neuroprotective effects under disease or stress. However, repeated stresses or lasting disease state may cause SNCA accumulation. Extraordinary upregulation of SNCA may be also harmful. Therefore, *SNCA* expression levels must be fine-tuned to maintain proper range *in vivo*. To clarify the regulatory mechanism of the ncRNA, with or without neurotoxic stresses, further intensive approach should be necessary.

In conclusion, our findings of the protective-allele specific YY1 and antisense ncRNA raised a novel possible mechanism to regulate *SNCA* expression.

CONFLICT OF INTEREST

The authors declare no conflict of interest.

ACKNOWLEDGEMENTS

We are grateful to the individuals with PD who participated in this study. We also thank Dr Yoshitaka Nagai for helpful comments; Dr Kouichi Ozaki for technical comments of luciferase assay and gel shift assay; Dr Fumiko Hirose and Dr Isao Kuraoka for technical comments of protein purification by affinity beads; Dr Hidetoshi Inoko and Dr Katsushi Tokunaga for control samples; Dr Yoshihisa Watanabe for technical comments of electroporation; and Dr Jennifer Logan for editing the manuscript. This work was supported by a grant from the Core Research for Evolutional Science and Technology (CREST), Japan Science and Technology Agency (JST); by the Global COE program and KAKENHI (17019044 and 19590990), both from the Ministry of Education, Culture, Sports, Science and Technology of Japan; and by the Grant-in-Aid for 'The Research Committee for the Neurodegenerative Diseases' of the Research on Measures for Intractable Diseases and Research Grant (H19-Genome-Ippan-001), all from the Ministry of Health, Labor and Welfare of Japan.

1 de Rijk, M. C., Tzourio, C., Breteler, M. M., Dartigues, J. F., Amaducci, L., Lopez-Pousa, S. *et al.* Prevalence of parkinsonism and Parkinson's disease in Europe: the EUROPARKINSON Collaborative Study. European Community Concerted Action on the Epidemiology of Parkinson's disease. *J. Neurol. Neurosurg. Psychiatry* **62,** 10–15 (1997).
2 Shults, C. W. Lewy bodies. *Proc. Natl Acad. Sci. USA* **103,** 1661–1668 (2006).
3 Farrer, M. J. Genetics of Parkinson disease: paradigm shifts and future prospects. *Nat. Rev. Genet.* **7,** 306–318 (2006).
4 Lesage, S. & Brice, A. Parkinson's disease: from monogenic forms to genetic susceptibility factors. *Hum. Mol. Genet.* **18,** R48–R59 (2009).
5 Warner, T. T. & Schapira, A. H. Genetic and environmental factors in the cause of Parkinson's disease. *Ann. Neurol.* **53** (Suppl 3), S16–S23 (2003).
6 Polymeropoulos, M. H., Lavedan, C., Leroy, E., Ide, S. E., Dehejia, A., Dutra, A. *et al.* Mutation in the α-synuclein gene identified in families with Parkinson's disease. *Science* **276,** 2045–2047 (1997).
7 Spillantini, M. G., Schmidt, M. L., Lee, V. M., Trojanowski, J. Q., Jakes, R. & Goedert, M. α -Synuclein in Lewy bodies. *Nature* **388,** 839–840 (1997).
8 Singleton, A. B., Farrer, M., Johnson, J., Singleton, A., Hague, S., Kachergus, J. *et al.* α -Synuclein locus triplication causes Parkinson's disease. *Science* **302,** 841 (2003).
9 Miller, D. W., Hague, S. M., Clarimon, J., Baptista, M., Gwinn-Hardy, K., Cookson, M. R. *et al.* α-Synuclein in blood and brain from familial Parkinson disease with *SNCA* locus triplication. *Neurology* **62,** 1835–1838 (2004).
10 Chartier-Harlin, M. C., Kachergus, J., Roumier, C., Mouroux, V., Douay, X., Lincoln, S. *et al.* α-Synuclein locus duplication as a cause of familial Parkinson's disease. *Lancet* **364,** 1167–1169 (2004).
11 Ibanez, P., Bonnet, A. M., Debarges, B., Lohmann, E., Tison, F., Pollak, P. *et al.* Causal relation between α-synuclein gene duplication and familial Parkinson's disease. *Lancet* **364,** 1169–1171 (2004).
12 Mueller, J. C., Fuchs, J., Hofer, A., Zimprich, A., Lichtner, P., Illig, T. *et al.* Multiple regions of α-synuclein are associated with Parkinson's disease. *Ann. Neurol.* **57,** 535–541 (2005).
13 Mizuta, I., Satake, W., Nakabayashi, Y., Ito, C., Suzuki, S., Momose, Y. *et al.* Multiple candidate gene analysis identifies *α-synuclein* as a susceptibility gene for sporadic Parkinson's disease. *Hum. Mol. Genet.* **15,** 1151–1158 (2006).
14 Satake, W., Nakabayashi, Y., Mizuta, I., Hirota, Y., Ito, C., Kubo, M. *et al.* Genome-wide association study identifies common variants at four loci as genetic risk factors for Parkinson's disease. *Nat. Genet.* **41,** 1303–1307 (2009).
15 Simon-Sanchez, J., Schulte, C., Bras, J. M., Sharma, M., Gibbs, J. R., Berg, D. *et al.* Genome-wide association study reveals genetic risk underlying Parkinson's disease. *Nat. Genet.* **41,** 1308–1312 (2009).
16 Bower, J. H., Maraganore, D. M., McDonnell, S. K. & Rocca, W. A. Incidence and distribution of parkinsonism in Olmsted County, Minnesota, 1976-1990. *Neurology* **52,** 1214–1220 (1999).
17 Adachi, O., Kawai, T., Takeda, K., Matsumoto, M., Tsutsui, H., Sakagami, M. *et al.* Targeted disruption of the *MyD88* gene results in loss of IL-1- and IL-18-mediated function. *Immunity* **9,** 143–150 (1998).

18 Ozaki, K., Ohnishi, Y., Iida, A., Sekine, A., Yamada, R., Tsunoda, T. *et al.* Functional SNPs in the lymphotoxin-α gene that are associated with susceptibility to myocardial infarction. *Nat. Genet.* **32,** 650–654 (2002).
19 Kuruma, H., Egawa, S., Oh-ishi, M., Kodera, Y., Satoh, M., Chen, W. *et al.* High molecular mass proteome of androgen-independent prostate cancer. *Proteomics* **5,** 1097–1112 (2005).
20 Rappsilber, J., Ishihama, Y. & Mann, M. Stop and go extraction tips for matrix-assisted laser desorption/ionization, nanoelectrospray, and LC/MS sample pretreatment in proteomics. *Anal. Chem.* **75,** 663–670 (2003).
21 Rylski, M., Amborska, R., Zybura, K., Konopacki, F. A., Wilczynski, G. M. & Kaczmarek, L. Yin Yang 1 expression in the adult rodent brain. *Neurochem. Res.* **33,** 2556–2564 (2008).
22 International Parkinson Disease Genomics Consortium, Nalls, M. A., Plagnol, V., Hernandez, D. G., Sharma, M., Sheerin, U. M. *et al.* Imputation of sequence variants for identification of genetic risks for Parkinson's disease: a meta-analysis of genome-wide association studies. *Lancet* **377,** 641–649 (2011).
23 Zabetian, C. P., Hutter, C. M., Factor, S. A., Nutt, J. G., Higgins, D. S., Griffith, A. *et al.* Association analysis of *MAPT* H1 haplotype and subhaplotypes in Parkinson's disease. *Ann. Neurol.* **62,** 137–144 (2007).
24 Stefansson, H., Helgason, A., Thorleifsson, G., Steinthorsdottir, V., Masson, G., Barnard, J. *et al.* A common inversion under selection in Europeans. *Nat. Genet.* **37,** 129–137 (2005).
25 Shi, Y., Lee, J. S. & Galvin, K. M. Everything you have ever wanted to know about Yin Yang 1..... *Biochim. Biophys. Acta* **1332,** F49–F66 (1997).
26 Gordon, S., Akopyan, G., Garban, H. & Bonavida, B. Transcription factor YY1: structure, function, and therapeutic implications in cancer biology. *Oncogene* **25,** 1125–1142 (2006).
27 Shrivastava, A. & Calame, K. An analysis of genes regulated by the multi-functional transcriptional regulator Yin Yang-1. *Nucleic Acids Res.* **22,** 5151–5155 (1994).
28 Fuchs, J., Tichopad, A., Golub, Y., Munz, M., Schweitzer, K. J., Wolf, B. *et al.* Genetic variability in the *SNCA* gene influences α-synuclein levels in the blood and brain. *FASEB J.* **22,** 1327–1334 (2008).
29 Linnertz, C., Saucier, L., Ge, D., Cronin, K. D., Burke, J. R., Browndyke, J. N. *et al.* Genetic regulation of α-synuclein mRNA expression in various human brain tissues. *PLoS One* **4,** e7480 (2009).
30 Kayano, M., Takigawa, I., Shiga, M., Tsuda, K. & Mamitsuka, H. Efficiently finding genome-wide three-way gene interactions from transcript- and genotype-data. *Bioinformatics* **25,** 2735–2743 (2009).
31 Wang, Y., Joseph, S. J., Liu, X., Kelley, M. & Rekaya, R. SNPxGE^2: a database for human SNP-coexpression associations. *Bioinformatics* **28,** 403–410 (2012).
32 Costa, F. F. Non-coding RNAs: meet thy masters. *Bioessays* **32,** 599–608 (2010).
33 Faghihi, M. A., Modarresi, F., Khalil, A. M., Wood, D. E., Sahagan, B. G., Morgan, T. E. *et al.* Expression of a noncoding RNA is elevated in Alzheimer's disease and drives rapid feed-forward regulation of β-secretase. *Nat. Med.* **14,** 723–730 (2008).
34 Modarresi, F., Faghihi, M. A., Lopez-Toledano, M. A., Fatemi, R. P., Magistri, M., Brothers, S. P. *et al.* Inhibition of natural antisense transcripts in vivo results in gene-specific transcriptional upregulation. *Nat. Biotechnol.* **30,** 453–459 (2012).
35 Chandra, S., Gallardo, G., Fernández-Chacón, R., Schlüter, O. M. & Südhof, T. C. α-synuclein cooperates with CSPα in preventing neurodegeneration. *Cell* **123,** 383–396 (2005).
36 Musgrove, R. E. J., King, A. E. & Dickson, T. C. Neuroprotective upregulation of endogeneous alpha-synuclein precedes ubiquitination in cultured dopaminergic neurons. *Neurotox. Res.* **19,** 592–602 (2011).

Supplementary Information accompanies the paper on Journal of Human Genetics website (http://www.nature.com/jhg)

J Neurol (2013) 260:1664–1666
DOI 10.1007/s00415-013-6916-0

LETTER TO THE EDITORS

A novel mutation in the C2 domain of protein kinase C gamma associated with spinocerebellar ataxia type 14

Takehiro Ueda · Tsuneyoshi Seki · Kimitaka Katanazaka · Kenji Sekiguchi · Kazuhiro Kobayashi · Fumio Kanda · Tatsushi Toda

Received: 30 January 2013 / Revised: 3 April 2013 / Accepted: 4 April 2013 / Published online: 21 April 2013

Dear Sirs,

Spinocerebellar ataxia type 14 (SCA14; Online Mendelian Inheritance in Man, OMIM #605361) is an autosomal dominant neurodegenerative disorder characterized by mild and slowly progressive cerebellar ataxia. Additional symptoms, including myoclonus, spasticity, dystonia, disturbance of deep sensation, and cognitive impairment, are observed in some patients [1, 2]. The SCA14 is caused by mutations in the *protein kinase C gamma* (*PRKCG*) gene (OMIM *176980), which encodes protein kinase C gamma (PKCγ). *PRKCG* contains 18 exons, and the PKCγ protein is composed of regulatory C1 and C2 domains and catalytic C3 and C4 domains. Most *PRKCG* mutations described till this date lie in the C1 domain [3, 4], while no mutations have been found in the C2 domain so far. Here we describe, for the first time, a mutation in the C2 domain in a patient with a typical SCA14 phenotype.

A 58-year-old Japanese woman visited our hospital with gait disturbance and lisping, the latter being noticed by her husband. At the age of 40, she frequently experienced unsteadiness. At the age of 55, she visited a clinic after experiencing a fall, and brain imaging revealed cerebellar atrophy. Her father suffered from gait disturbance and dysphagia in his late 70s, and her father's brother (the patient's uncle) and his nephew (the patient's cousin) had an unsteady gait. This family history indicated autosomal dominant inheritance (Fig. 1a).

T. Ueda (✉) · T. Seki · K. Katanazaka · K. Sekiguchi · K. Kobayashi · F. Kanda · T. Toda
Division of Neurology/Molecular Brain Science, Kobe University Graduate School of Medicine, 7-5-1, Kusunoki-chou, Chuo-ku, Kobe 650-0017, Japan
e-mail: taueda@med.kobe-u.ac.jp

Neurological examination revealed cerebellar ataxia, including slurred speech, saccadic eye movement, and limb and truncal ataxia. Although there was a mild decrease in the deep sensations in her lower limbs, her gait disturbance was mostly consistent with ataxic gait. At her first visit to our institution, she had a score of 27/100 on the International Cooperative Ataxia Rating Scale. Blood, respiratory function, and cerebrospinal fluid tests yielded no remarkable findings. Brain magnetic resonance imaging demonstrated cerebellar atrophy, particularly in the upper part (Fig. 1b), and *N*-isopropyl-*p*-[123I]-iodoamphetamine single-photon emission computed tomography revealed decreased blood flow only in the upper cerebellum. She had no autonomic failure or cognitive dysfunction. Clinically, her symptoms corresponded with typical SCA14 features.

While she had a family history of autosomal dominant inheritance, genetic testing for SCA types 1, 2, 3, 6, 7, 8, and 31 and dentatorubral–pallidoluysian atrophy, genes relatively frequent in Japan, did not show the presence of abnormal alleles. Next, to test for mutations in *PRKCG*, we performed genomic PCR followed by a direct sequencing analysis. This revealed the presence of the single-base substitution c.518T>G in exon five involving amino acid change p.Ile173Ser (Fig. 1c). This substitution has not been reported, either as a single-nucleotide polymorphism or as a mutation. The amino acid p.Ile173 residue is conserved among PRKCG proteins from mammals and zebrafish (Fig. 1d). To ascertain whether this was a disease-associated mutation, we first performed direct sequencing of this region in 200 Japanese healthy controls and found that none of them carried this alternative allele. Next, we employed three computer algorithms to predict the effect of this novel mutation: Sorting Intolerant From Tolerant (SIFT, http://sift.bii.a-star.edu.sg/), Polymorphism Phenotyping v2